DIAGNOSTICS FOR INTENSE PULSED ION BEAMS

NAVAL RESEARCH LABORATORY
WASHINGTON, D. C.

OCTOBER 1976

365117

Diagnostics for Intense Pulsed Ion Beams

F. C. YOUNG

Radiation Detection Group
Radiation Technology Division

and

J. GOLDEN AND C. A. KAPETANAKOS

Experimental Plasma Physics Branch
Plasma Physics Division

October 1976

DDC

RECEIVED

DEC 27 1976

A

NAVAL RESEARCH LABORATORY
Washington, D.C.

REPORT DOCUMENTATION PAGE		READ INSTRUCTIONS BEFORE COMPLETING FORM
1. REPORT NUMBER NRL Memorandum Report 3391	2. GOVT ACCESSION NO.	3. RECIPIENT'S CATALOG NUMBER
4. TITLE (and Subtitle) DIAGNOSTICS FOR INTENSE PULSED ION BEAMS		5. TYPE OF REPORT & PERIOD COVERED Interim report on a continuing NRL problem.
		6. PERFORMING ORG. REPORT NUMBER
7. AUTHOR(s) F.C. Young, J. Golden and C.A. Kapetanakos		8. CONTRACT OR GRANT NUMBER(s)
9. PERFORMING ORGANIZATION NAME AND ADDRESS Naval Research Laboratory Washington, D.C. 20375		10. PROGRAM ELEMENT, PROJECT, TASK AREA & WORK UNIT NUMBERS NRL Problem H02-28A
11. CONTROLLING OFFICE NAME AND ADDRESS Office of Naval Research Arlington, Virginia 22217		12. REPORT DATE October 1976
		13. NUMBER OF PAGES 62
14. MONITORING AGENCY NAME & ADDRESS(if different from Controlling Office)		15. SECURITY CLASS. (of this report) UNCLASSIFIED
		15a. DECLASSIFICATION/DOWNGRADING SCHEDULE

16. DISTRIBUTION STATEMENT (of this Report)

Approved for public release; distribution unlimited.

17. DISTRIBUTION STATEMENT (of the abstract entered in Block 20, if different from Report)

18. SUPPLEMENTARY NOTES

19. KEY WORDS (Continue on reverse side if necessary and identify by block number)

Plasma physics
Relativistic electron beam technology
Intense ion beams
Plasma diagnostics

20. ABSTRACT (Continue on reverse side if necessary and identify by block number)

Diagnostic methods and techniques for intense pulsed ion beams are presented. Especially important is a detailed description of the measurement of delayed radioactivity from nuclear reactions induced in a target by the ions. This activation analysis provides the most precise, un-ambiguous means of determining the number of ions per pulse that is presently available. A com-pilation of yields and cross sections for several nuclear reactions is given. Included among the nuclear techniques is the measurement of prompt radiation such as gamma-rays and neutrons

(Continued)

DD FORM 1473 EDITION OF 1 NOV 65 IS OBSOLETE   i
1 JAN 73
S/N 0102-014-6601

20. Abstract (Continued)

from ion induced reactions. In addition a scintillator-photodiode detector is described which has been proven to be useful for the measurement of time-of-flight and which may be used to observe the relative pulse shape. Biased ion collectors and difficulties associated with their use are also discussed.

CONTENTS

iii

DIAGNOSTICS FOR INTENSE PULSED ION BEAMS

I. INTRODUCTION

Within the last two years the production of intense pulsed ion beams has advanced from beams of current density, $J_i \sim 10$ A/cm^2 with peak ion currents $I_p \sim 0.5$ kA at 150 keV energies[1] to ultra-high-power ($> 10^{11}$ W) beams with $J_i > 1$ kA/cm^2 and $I_p > 200$ kA, containing more than 4×10^{16} ions per pulse[2,3] at energies of 1 MeV. This report is about the diagnostic techniques and methods used to analyze these intense ion beams.

Determination of the parameters of an intense ion beam is more difficult than for a relativistic electron beam for which a plethora of techniques has been developed. In part, this is due to the fact that intense ion beams are generally space-charge and current neutralized. These traits preclude many electrical measurements involving charge collection or the measurement of self-magnetic fields. It also makes uncertain the use of ion spectrometers.

Presently, the most unambiguous method for the determination of the identity, number and spatial distribution of light ions is by nuclear activation of a target.[4] Another useful tool, a scintillator monitored by a fast photodiode, can be used to measure time-of-flight and, if the particle energies are approximately known, also yields information about the pulse shape. In fact, by using masks of various thicknesses less

---

Note: Manuscript submitted October 6, 1976.

1

than a particle range, the energy can be approximately determined. In combination, these two diagnostic methods furnish information about the current of the ion pulse.[4]

In the following discussion, the details of these two diagnostic methods are presented. The application of Faraday cups is also described, although this technique can only be used with some degree of certainty when a transverse magnetic field is present inside the Faraday cup.

II. NUCLEAR ACTIVATION TECHNIQUES

When a pulse of energetic ions strikes a suitable target, a small fraction of the ions induces nuclear reactions in the target. If the cross-section for a given reaction is known, then the number of incident ions in the pulse can be determined from a measurement of the decay of any radioactive reaction products or by the detection of any prompt radiation. Observation of the prompt radiation -- typically neutrons, gamma-rays, protons, or alpha particles -- is usually difficult because the signal to background ratio is very small. However, for ions of the light elements, there are a number of reactions which produce radioactive nuclei that decay with half-lives of a few minutes by emitting positrons. Coincident counting the pair of gamma-rays associated with the annihilation of the positrons offers an extremely sensitive means of detecting a relatively small number of reactions. In particular, this discussion shall concentrate on the (p,γ) and the (d,n) reactions with ^{10}B, ^{12}C and ^{14}N targets because ultra-high power, intense beams of protons and deuterons have already been produced in the laboratory. These

2

reactions are listed in Table I with the half-lives of the reaction products. (A cursory summary of reactions for other ions is also given below.) Because the cross-sections for these reactions are fairly well known, a relatively precise determination of the ion number/pulse can be made. Moreover, since the ions are required to have a minimum energy for the reaction to occur, this method is insensitive to low energy ions. Thus, there is no interference from low energy plasma or debris that might strike the target.

There are two complications which occur when using nuclear activation analysis of high power, high current density beams. One is interference from different ions causing reactions which produce the same radioactivity. For example, in proton beams there may be a small quantity of deuterium present in the proton source. Although the natural abundance of deuterium is 1.5×10^{-4}, the (d,n) reaction yields are of the order of 10^4 times greater than the (p,γ) reaction yields. To separate the contributions of the two components of the beam either different material targets must be used or the relative abundance of protons and deuterons must be known. The second complication is caused by the loss of reaction products due to heating and evaporation of the surface of the target by the intense beam. Typically, the radioactive nuclei are produced a few microns into the target. This target "blow-off" can be avoided by attenuating the ion beam with metal screens of known transmission.

3

II.1 Detection Apparatus for Coincidence Counting

It is presently possible to detect as few as 100 radioactive nuclei produced by the reactions listed in Table I. To do this, standard commercial electronic instrumentation can be used to perform both pulse-height discrimination and coincidence counting so that only 0.51 MeV gamma-rays from the positron annihilation are detected. A block diagram of the apparatus is shown in Fig. 1.

After activation, the target is placed between two NaI(Tl) crystals which are coupled to photomultiplier tubes. Each pulse is amplified by a double-delay-line (DDL) amplifier which provides a bipolar pulse with a fast crossover at a precise time. Pulse height analysis is then performed by a fast timing single-channel-analyzer (SCA) which gives an output pulse only if the input pulse amplitude is between two adjustable values (pulse-height window). Also this output pulse is precisely timed relative to the fast crossover of the input pulse. The output of one SCA is delayed (typically 50 ns). The earlier SCA output then starts a time-to-amplitude converter of a time analyzer (a time-to-amplitude converter and SCA) which is then stopped by the delayed timing-SCA output. If the time interval between the start and stop commands is within a specified time window (e.g., 100 ns) then the SCA of the time analyzer is triggered to produce an output pulse which is counted by a scaler. The sample is counted for a present time.

To optimize the coincidence counting, the NaI crystals should be placed as close together as possible aligned at 180° to each other. This provides the maximum solid angle for intercepting gamma-ray pairs by the crystals. Because the response of the detector depends on the radial

4

position of the source from the cylindrical axis of the NaI(Tl) crystals, the crystals should be much larger than the activated target. (3" dia. and 5" dia. are commercially available). The thickness of the crystals should be chosen for optimum response to 0.511 MeV gamma-rays (e.g., NaI thickness 2" to 3"). The crystals and photomultipliers must be shielded from background radiation such as cosmic ray showers and other environmental radiation. A few inches of lead is generally sufficient. If the apparatus is in the neighborhood of high power pulsed high voltage generators, it is also necessary to shield the PM tubes and their preamplifier output cables from electromagnetic inteference. Magnetic shielding of the PM tubes is recommended to minimize the effect of stray magnetic fields. Moreover, to prevent a drift of the amplifier gains, the electronics should be protected from temperature fluctuations.

The detection apparatus may be absolutely calibrated with a positron emitting source of known activity. For example, 90% of the decays of ^{22}Na are by positron emission and 10% are by electron capture. A 1 μCurie source is sufficient to provide about 3×10^4 positrons/second. A typical detection efficiency is 5% yielding 1.5×10^3 counts/sec. To set the pulse-height windows on the timing-SCA's, an oscilloscope, triggered by the output of the SCA, is used to monitor the DDL amplifier output (or if available, the DL output of the DDL amplifier). Thus that part of the pulse height spectrum which triggers the timing SCA is observed; the windows can be set on the 0.511 MeV peaks and narrowed to an appropriate width (e.g. ± 50 keV).

II.2 Analysis

The number of radioactive nuclei N_0 produced via a nuclear reaction of cross section σ by N particles of energy E incident on a target of thickness Δx with n target nuclei/cm^3 is given by $N_0(E) = N\sigma(E) n \Delta x$ providing that the thickness Δx is sufficiently small so that E does not change appreciably as the particles transverse the target. The reaction characteristics of this expression can be consolidated into a reaction yield given by $dY = \sigma(E) ndx$ where dx is a differential target thickness. If this yield is known and N_0 is experimentally measured, the number of incident particles can be determined.

For measurements with intense pulsed beams, thick targets are used. The targets are thicker than the range of the incident particles. Therefore, the reaction yield must be integrated over the target thickness ℓ in order to obtain the thick target yield,

$$Y(E_i) = \int_0^\ell \sigma(E) \, ndx = n \int_0^{E_i} \frac{\sigma(E)}{\left|\frac{dE}{dx}\right|} \, dE = \int_0^{E_i} \frac{\sigma(E)}{\epsilon(E)} \, dE , \tag{1}$$

where E_i is the incident energy of the ions and $\epsilon(E) = \frac{1}{n}\left|\frac{dE}{dx}\right|$ is the stopping cross section. The stopping cross section is a slowly varying function of energy so that this expression for $Y(E_i)$ can be evaluated by numerical integration if the cross section is known. For (d,n) reactions at low energy the cross sections are rapidly increasing with energy and numerical integrations are readily carried out. For resonance reactions, such as (p,γ) reactions, the resonant behavior of the cross section simplifies the evaluation of the integral in Eq. (1).

6

The cross section of a resonance reaction is peaked at the resonance energy E_R. The cross section in the vicinity of a resonance of width Γ is given by

$$\sigma(E) = \frac{\Gamma^2}{4} \frac{\sigma_R}{(E - E_R)^2 + \Gamma^2/4} , \tag{2}$$

where σ_R is the cross section at the peak of the resonance. For a resonance with a narrow width, Eq. (1) may be approximated by

$$Y = \frac{1}{\epsilon(E_R)} \int_0^\infty \sigma(E) dE = \frac{1}{\epsilon} \frac{\pi}{2} \sigma_R \Gamma , \tag{3}$$

provided the ion energy is well above the resonance energy, i.e., $(E_i - E_R) \gg \Gamma$. The quantity $Y_\infty = \pi \sigma_R \Gamma / 2\epsilon$ is called the "thick-target step" of a resonance. This quantity is characteristic of a particular nuclear reaction resonance and target composition. In this case the number of incident particles with energies greater than the resonance energy is given by $N = N_0/Y_\infty$

For a mixed beam of protons and deuterons, the number of radioactive nuclei induced in the "target" is given by

$$N_0 = Y_p N_p + \int Y_d(E) \frac{dN_d}{dE} dE , \tag{4}$$

where Y_p is the (p,γ) resonance thick-target step, and N_p is the number of protons with energy greater than the resonance energy. If the deuteron component of the beam is mono-energetic, or if the yield from the (d,n) reaction is approximately independent of energy over the energy

spread of the deuteron beam, then

$$N_o = Y_p N_p + Y_d N_d .$$ (5)

If the fraction of deuterons in the beam is known, (e.g., an isotopic abundance, $N_d/N_p = 1.5 \times 10^{-4}$), then N_p is given by

$$N_p = N_o \left(Y_p + \frac{N_d}{N_p} Y_d \right)^{-1} .$$ (6)

The number of radioactive nuclei is determined by measuring the induced activity as described in Section II.1. During the time interval t_1 between activation and the beginning of counting, some of the radioactive nuclei decay. The fraction of nuclei remaining after a time t_1 is given by $\exp(-t_1/\tau)$ where τ is the lifetime. If the activity is measured for a time interval, $\Delta t = t_2 - t_1$, beginning at a time t_1, the fraction of nuclei present at t_1 which decays during this interval is $[1 - \exp(-\Delta t/\tau)]$. Of these decays, the detector measures only a fraction $\hat{\epsilon}$ given by the efficiency of the detector. Therefore the number of counts tallied is

$$k = \hat{\epsilon} \, e^{-t_1/\tau} \left(1 - e^{-\Delta t/\tau} \right) N_o ,$$ (7)

and the number of protons in the beam is given by

$$N_p = k \, e^{t_1/\tau} \left[\left(1 - e^{-\Delta t/\tau} \right) \left(Y_p + \frac{N_d}{N_p} Y_d \right) \hat{\epsilon} \right]^{-1} .$$ (8)

A similar equation results for deuteron beams containing a small fraction of protons. However, in this case N_p/N_d must be determined by other means, such as comparison with other reactions or theoretical

8

considerations. Often it is very difficult to measure a small flux of protons in the presence of a large flux of deuterons since the deuteron yield is much larger than the proton yield.

II.3 Evaluation of Reaction Yields

Reactions yields for thick targets may be calculated according to Eq. (1) if the cross sections are known as a function of energy. However the integration of the cross sections is not necessary for several (p,γ) reactions because there are experimental measurements of the thick target steps. The following sections are devoted to evaluations of the reaction yields for several different reactions.

When measurements are made on targets of different compositions, the stopping cross sections must be appropriately corrected. For targets of chemical formula $X_a Y_b$, the composition rule[6] is $\epsilon = a\,\epsilon_x + b\,\epsilon_y$, where ϵ_x and ϵ_y are the atomic-stopping-cross-sections. Some proton stopping cross sections are given in Figs. 2 & 3 from curves by Demirlioglu and Whaling.[5] These curves can be used for deuterons by noting that the stopping-cross-section for a deuteron of energy 2E is equal to that of a proton of energy E.

(a) $\quad {}^{12}C(p,\gamma){}^{13}N(\beta^+){}^{13}C$
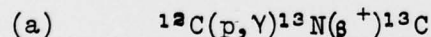
This reaction[7] has a resonance at 0.457 MeV with $\Gamma = 37$ keV and a resonance at 1.698 MeV with $\Gamma = 67$ keV. The yield of positrons from this reaction with protons of energy up to 2.5 MeV on a thick natural carbon target has been measured by Seagrave.[8] The thick target step of the 0.46 MeV resonance is $(7.5 \pm 0.5) \times 10^{-10}$ ^{13}N/proton (measured at 1 MeV).

9

The step of the 1.70 MeV resonance is 1.45 ± 0.03 times that of the lower resonance. A thick-target step for the 0.46 MeV resonance $\frac{1}{3}$ smaller than the value above is deduced from the measurements of Reiss, et al.[9] The useful energy range of this reaction to avoid the high energy resonance is from 0.6 to 1.5 MeV as shown in Fig. 4. The only major interference reaction is $^{12}C(d,n)^{13}N$ which is discussed in Section (d) below.

(b) $^{14}N(p,\gamma)^{15}O(\beta^{+})^{15}N$
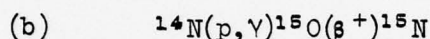
Below 2 MeV this reaction has five resonances.[7] The resonance energies, half-widths and thick-target yields are given in Table II. The thick target yields are calculated for resonance parameters taken from Ref. 7. For the 0.278 MeV resonance, Hebbard and Bailey[10] compare thick-target yields measured by a number of investigators corrected to a pure atomic nitrogen (N) target. Their measurement gives $Y = (2.1 \pm 0.3) \times 10^{-11}$ ^{15}O/proton which is in good agreement with the value calculated in Table II. For a practical target such as boron nitride (BN) the yield from atomic nitrogen must be multiplied by the ratio of the stopping cross sections in nitrogen to the stopping cross section in BN, i.e., $\epsilon_{N}/\epsilon_{BN} \sim 0.56$. The computed thick-target steps for each resonance for a BN target are given in Table II. Also the total yield for this reaction between any two resonances for a thick BN target is given in the right hand column of Table II.

(c) $^{10}B(p,\gamma)^{11}C(\beta^{+})^{11}B$
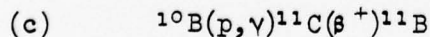
The cross section for this reaction below 2 MeV has been measured in three independent laboratories.[11-13] This reaction has a broad resonance

($\Gamma = 500 \pm 50$ keV) at 1.145 MeV proton energy.[14] The most accurate and complete cross sections are reported by Chadwick, Alexander, and Warren[13] and their absolute cross section is displayed in Fig. 5. To determine the thick target yield for this reaction it is necessary to carry out the integration described in Eq. (1). If a BN target is used, the stopping cross section for BN must be evaluated and weighted by the isotopic abundance of ^{10}B, $\xi(^{10}$B$) \sim 19.8\%$. Yields computed by integrating the cross sections of Chadwick et al.[13] combined with stopping cross sections obtained from Ref. 5 are listed in Table III.

(d) ^{10}B$(d,n)^{11}$C$(\beta^+)^{11}$B
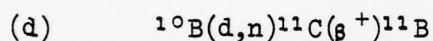
Cross sections for neutron emission from this reaction have been measured in the forward direction from 0.2 to 2 MeV by Burke et al.[15] and from 0.3 to 4.5 MeV by Marion et al.[16] These results are consistent with each other. For deuterons with energies above 1.9 MeV, the neutron cross sections may not be a good measure of positron production because the reaction can produce particle unstable levels of ^{11}C. The measurements below 2 MeV can be converted to total cross sections using the angular distributions of Ref. 15 at 0.71, 1.06 and 1.43 MeV deuteron energy. Based on these distributions, conversion of the measured forward angle cross sections (σ_e) of Ref. 15 to total cross sections (σ_t) are estimated to be $\sigma_t/4\pi\sigma_e = 0.55$. The thick-target yield for this reaction with a BN target was calculated according to Eq. (1). The results are given in Fig. 6 and Table IV. Also stopping cross sections for BN are listed to facilitate converting these yields to other target materials.

The thick-target yield for this reaction on a BN target has been measured from 0.5 to 3.2 MeV by measuring the induced positron activity and cross sections have been inferred from the thick-target yields.[17] The yields and cross sections are in agreement with the results presented in Table IV within experimental error. However, the results of Ref. 17 were not used in the evaluation of cross sections and thick target yields for the $^{10}B(d,n)^{11}C$ reaction because differences have been observed with similar comparisons for other reactions measured by the same investigators. In particular, cross sections for the $^{27}Al(d,p)^{28}Al$ reaction reported by Schuster and Wohlleben[18] are an order of magnitude larger than cross sections measured in three independent experiments.[19] Also, cross sections and thick-target yields for the $^{14}N(d,n)^{15}O$ reaction of Wohlleben and Schuster[17] are 2 to 3 times larger than values determined in two different experiments as described in the next section. Because these unexplained differences exist, results of Wohlleben and Schuster have not been used in evaluating cross sections and thick-target yields.

(e) $^{14}N(d,n)^{15}O(\beta^+)^{15}N$
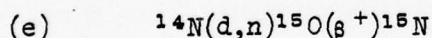
This reaction has been studied below 700 keV deuteron energy by direct measurements of the positron activity.[20] The reaction has an apparent threshold of 143 keV presumably because at low energy the reaction proceeds primarily through the first two excited states of ^{15}O rather than the ground state. From 170 to 700 keV the thick-target yield is observed to increase by six orders of magnitude. Measurements of the neutron production at high energy indicate that the cross section continues

to rise to a value of about 20 mb at 2 MeV and then flattens off.[31] Because of its small cross section at low energy this reaction does not appear to be very useful for energies below 700 keV. Above 2.5 MeV deuteron energy, neutron cross sections may not be a good measure of positron production because the reaction can lead to proton unstable levels of excitation in ^{15}O. The thick-target yield for this reaction with a BN target calculated from the measurements of Refs. 20 and 21 are given in Table V and plotted in Fig. 7.

(f) $^{12}C(d,n)^{13}N(\beta^+)^{13}C$
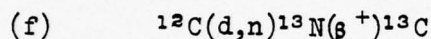
This reaction has a threshold at 328 keV deuteron energy and the cross section for the production of ^{13}N positron activity has been measured from just above threshold to 1.85 MeV.[22,23] From 2.0 to 5.0 MeV precise measurements of the total cross sections and thick-target yields have been reported by Jaszczak et al.[24] The uncertainty of the latter measurements, which are based on the number of neutrons observed by a 4π-detector is estimated to be ± 3%. Above 3.0 MeV neutron cross sections may not be a good measure of positron production because the reaction can lead to proton unstable levels in ^{13}N. The cross sections below 2 MeV have been used to calculate the shape of the thick-target yield which is listed as "Relative Yield" in Table VI. The 90° cross sections of Ref. 25 from 1.8 to 2.4 MeV have been normalized to these cross sections in order to extend this relative thick-target yield above 2 MeV. Then this yield is normalized to the precision measurements of Ref. 24 to give the "Absolute Yield" in Table VI and the thick-target yield in Fig. 8.

13

II.4 Proton and Deuteron Beams on BN Targets and Carbon Targets

When a proton or deuteron beam strikes a BN target, both ^{15}O and ^{11}C may be produced. In order to unscramble these two radioactive products, the decay is monitored as a function of time. Since ^{15}O decays an order of magnitude faster than ^{11}C, the long time activity of the target is due mainly to ^{11}C. The contribution of ^{15}O can be determined by fitting the activity as a function of time to a decay curve with a slope corresponding to the lifetime of ^{11}C for times greater than a few lifetimes of ^{15}O. The ^{11}C is then subtracted from the total activity. An example is shown in Fig. 9 taken from Golden and Kapetanakos.[36]

Due to the isotopic abundance of deuterium, proton beams extracted from a plasma produced from hydrogenic materials always contain a small component of deuterons. For an accurate determination of the number of protons per pulse, it is necessary to correct the activity of the target for the contribution from deuteron induced reactions. It has been shown (Section II.2) that the number of counts due to a given reaction is proportional to $\left[Y_p + \dfrac{N_d}{N_p} Y_d \right]$, where N_d/N_p is the ratio of the number of deuterons to protons per pulse. The deuteron correction is made assuming that in an ion source operating in the space-charge limited regime, the current density of the various singly-ionized species is proportional to their relative abundance divided by the square-root of their mass. Specifically, if a proton beam is extracted from a hydrogenic material in which the isotopic abundance of deuterium is $\xi(D)$, the ratio of deuteron current density to that of protons is $J_d/J_p \sim \xi(D)/\sqrt{2}$. Therefore,

14

the deuteron correction is made by calculating the energy dependent factor, F, defined as

$$F = Y_p \left[Y_p + \frac{\xi(D)}{\sqrt{2}} Y_d \right]^{-1}. \tag{9}$$

Equation (8) then becomes

$$N_p = k \, e^{t_1/\tau} \left[\left(1 - e^{-\Delta t/\tau} \right)_{\hat{\epsilon}}^{\wedge} Y_p \right]^{-1} F. \tag{10}$$

The factor, F, is plotted in Figs. 10-12 for BN and graphite targets.

II.5 "Blow-Off"

The loss of radioactive nuclei from the target prior to counting is called "blow-off". Apparently this is not due to diffusion out of the target in the course of a few seconds[2] but rather is the result of intense heating of the target surface on a short time scale.

As an example of the importance of the correction, consider a carbon target for a 60 ns duration, 1 kA/cm^2 pulse of 900 keV protons. The power input per unit area is 9×10^{12} W/m^2, corresponding to an energy dose of 5.4×10^5 J/m^2. The energy deposition depth, for normal incidence is equal to the proton range, i.e., ~ 11 μm. Most of the activation, however, occurs in the first 6.6 μm from the surface. Because thermal conduction times are microseconds and shock speeds are a few 10^3 m/s, almost all of the energy deposited near the surface remains during the lifetime of the pulse. Since carbon has a heat capacity, $C_p \sim 20$ J/mole $^\circ$K, and sublimation[27] takes place at 3350°K with a heat of sublimation, $\Delta H_s \sim 7.12 \times 10^5$ J/mole, 1.1×10^5 J/m^2 are required to raise an 11 μm surface layer to the sublimation temperature.* This

15

leaves ~ 4.3×10^5 J/m^2, enough to remove a 3.6 μm thick layer, over one-half of the activation depth. Therefore, it might be expected that a large fraction of the reaction products can be lost from the target.

However, the "blow-off" does not appear to be a limitation to the usefulness of the activation technique because it can easily be avoided by attenuating the ion beam using metal screens of known transmission. In fact, if the beam is sufficiently uniform or reproducible, comparison of target-activations with and without attenuating screens provides a method for the determination of the importance of "blow off".[2]

II.6 Ion Diagnostics by Neutron Production

Ion intensities can be determined by measuring neutrons produced by nuclear reactions induced by an intense pulse of ions. A variety of reactions that have been used in this way are listed in Table VII. Usually a thick sample of the target material is placed in vacuum and irradiated by the ion pulse. Neutrons are then detected outside the vacuum system with a neutron activation detector.[37] Since many of these reactions also produce short-lived activations, measurements of both the neutron output and the delayed activity can provide a consistency check on ion intensity determinations.

The $D(d,n)^3He$ reaction is of particular interest because it is useful at ion energies below 1 MeV and has been used by many investigators. Cross sections for the $D(d,n)^3He$ and $D(d,p)T$ reactions have been measured by a number of investigators[28,38,39] and are shown in Fig. 13. The thick-target yield of the $D(d,n)^3He$ reaction is given in Fig. 14 for

_____

* Within one range of the surface there are 1.8 moles/m^2.

16

a CD_2 target; the atomic stopping cross sections were obtained from
Ref. 5.

Although this neutron yield technique is experimentally simple, it
is considerably less accurate and reliable than the activation technique.
The ion energies must be known accurately because the neutron reaction
cross sections are energy dependent. Also cross sections for some
of the reactions in Table VII are only poorly known. Accurate calibra-
tion of a neutron detector is difficult because the calibration depends
on the neutron energy and should be made in situ on the plasma device.[37]
Furthermore, since the neutron reaction cross sections may vary with the
direction of emission of the neutrons, corrections for the neutron detec-
tor geometry may be necessary. Finally, ions from the plasma device may
bombard material other than the target of interest and produce neutrons
from unexpected reactions.

II.7 Ions With Energies Above 1.5 MeV

Above 1.5 MeV, a variety of nuclear reactions can be used for ion
diagnostics. The (p,n) reactions are attractive because the reactions
usually have a threshold energy in the range of a few MeV. In Table VIII
are listed examples of such reactions leading to relatively short-lived
reaction products which emit gamma-rays. Cross sections for these reac-
tions have been measured and the sources are listed in the table. These
reactions have the disadvantage that just above threshold the reaction
yield is rapidly increasing with energy so that it is rather difficult
to deduce ion intensities without knowing the ion energy distribution.

For deuterons of several MeV energy, there are several (d,p) and

(d,n) reactions which result in delayed gamma-ray activity. These reactions usually do not have a threshold energy, but the reaction is inhibited at low energy due to the Coulomb barrier. Examples of such reactions are listed in Table IX with the associated gamma-ray and half-life. Targets for the reactions in Table IX are readily available in nearly single isotopic composition thereby greatly reducing the possibility of interferences from competing reactions. Unfortunately cross sections and thick-target yields for these reactions leading to the desired delayed gamma-ray activities have not been measured extensively. Limited measurements have been used to calculate thick-target yields for these reactions on carbon and aluminum.[19] Simultaneous measurements with the reactions on carbon and aluminum have been used to determine mean deuteron energies. Thick-target yields for the $^{12}C(d,n)^{13}N$ and $^{27}Al(d,p)^{28}Al$ reactions and the ratio of ^{13}N to ^{28}Al are shown in Fig. 15 as given by Young and Friedman.[19]

Ions with energies in the 10 to 100 MeV range can be diagnosed using (p,xn) or (α,xn) reactions, where x = 1, 2, 3, ... These reactions can provide information on the ion intensity and energy distribution simultaneously. A good example of this kind is the $^{197}Au(\alpha,xn)^{201-x}Tl$ reactions to diagnose 20 to 70 MeV α-particles. Cross sections for these reactions,[41] as given in Fig. 16, are quite large ($\sim$ 1 barn), and the single isotopic Au target eliminates interferences from competing reactions. Each of these reactions produces a radioactive Tl nucleus which is a delayed gamma-emitter. The half-life, gamma-ray energy and branching ratio are listed in Table X. The gamma-ray intensities resulting from different (α,xn) reactions induced in a

18

thick Au target can be measured simultaneously with a high resolution
Ge-spectrometer of known absolute efficiency. Then α-particle in-
tensities are determined using the cross sections and decay properties.
Since the cross section for each (α,xn) reaction provides a window into
the α-particle energy spectrum (see Fig. 16), thick-target yields for
each reaction can be unfolded to determine the energy spectrum. It is
estimated that measurements can be made on a source of only ~ 10^8 α-
particles by counting with a high efficiency (~ 1% at 0.5 MeV) Ge-
spectrometer.

II.8 Detection of Prompt Gamma-Rays From the (p,γ) Reactions

The lack of time resolution is an important limitation of the nu-
clear activation technique, i.e., the number of ions per pulse is deter-
mined rather than the current. A possible means of measuring the proton
current is by monitoring the flux of gamma-rays which is emitted from
the (p,γ) reactions. Because such a measurement is done on the time
scale of the beam pulse duration, it is·expected that errors resulting
from "blow-off" will not be significant.

As stated in the beginning of Sect. II, observation of these prompt
gamma-rays is extremely difficult because of the copious burst of x-rays
from high energy electron bremsstrahlung produced in the ion source (re-
flex triode, pinched e-beam diode, etc.) This x-ray flux is generally
many orders of magnitude more powerful than that of gamma-rays from re-
actions in the target. For example, a 0.1 MA, 1 MeV proton beam on a
carbon target produces 4.7×10^{14} gamma-rays per second with 2.4 MeV

19

energy corresponding to a power of only 180 W. Fortunately, discrimination between target gamma-rays and bremsstrahlung may be possible by spatial collimation and by gating the gamma-ray detector. The use of collimation alone is probably inadequate to eliminate the interference by x-rays because even the small fraction of photons that scatter is sufficient to obscure the target gamma-rays. However, by placing the target far enough downstream so that time-of-flight is greater than the duration of the bremsstrahlung pulse, the target gamma-rays may be observable without interference. Furthermore, gating techniques[42] are available so that a detector consisting of a fast photo-diode or photo-multiplier tube can be switched-on before the ion beam reaches the target so that saturation of the detector by the x-rays is avoided. Experiments to demonstrate this diagnostic technique are presently underway.

III. SCINTILLATOR-PHOTODIODE DETECTOR

A useful tool for measurement of time-of-flight is a detector consisting of a thin scintillator (such as NE 102 or Pilot B) monitored by a fast photodiode. A schematic of such a device is shown in Fig. 17. In order to shield the scintillator from extraneous light, the scintillator face is coated with a vapor deposited layer of aluminum 0.2 - 1.5 μm thick. Typically, for current densities greater than a few hundred A/cm^2, screens must be used to attenuate the beam and prevent the aluminum from being blown off the scintillator.

To minimize the interference of gamma-rays, the scintillator is optically coupled to the photodiode by a long light-pipe consisting of an

acrylic rod encased in an electrically grounded stainless steel tube. Thin lead sheet is wrapped around the tube to reduce any scintillation in the acrylic light-pipe. Silicone grease is used to improve the coupling at the ends of the light-pipe. The aluminized surface of the scintillator is connected to the grounded stainless steel tube to prevent electrostatic charging. The tube is mounted in a sliding-seal feed-through so that the scintillator may be placed at various axial positions within the vacuum chamber.

From the time-of-flight measured at two axial positions, the particle velocity can be determined. For monoenergetic ions, the ratio q/m can readily be obtained from the measured velocity and the known value of the accelerating potential applied to the anode.

The energy distribution of the ions may be approximately determined by using filters a fraction of a range thick in front of the scintillator. This measurement requires many different thickness filters for any accuracy. Moreover, the response of the scintillator as a function of ion energy must be taken into account. For example, the response[43] of Pilot B and NE-102 scintillators is proportional to $E^{1.6}$ as shown in Fig. 18.

It is frequently convenient to use filters made of materials such as plastic polymers for which the ion range-energy curve is not readily available. The difficulty can be overcome by using the Bragg-Kleeman rule to compute the range, R, as follows,

$$\frac{R}{R_0} = \frac{\rho_0}{\rho} \left[\frac{A_{eff}}{A_0} \right]^{\frac{1}{2}} , \tag{11}$$

21

where

$$\sqrt{A_{eff}} = \sum_s n_s A_s \bigg/ \sum_s n_s \sqrt{A_s} \, .$$

In these equations, R_0, A_0 and ρ_0 are the range, atomic mass and the density of a material with known range and A_s and n_s are the atomic weight and mole-fraction of the sth component of the mixture with density ρ. Table XI lists the ratios of the range of protons in a number of common polymers to that in aluminum obtained using the Bragg-Kleeman rule. Figure 19 shows the range-energy curves for protons in aluminum, carbon ($\rho = 2.0$ gm/cm^3), polyethylene, and polyester (Mylar).[44]

The relative contribution of ions, electrons, and protons can be found by using filters in front of the scintillator. Relevant data on x-ray absorption coefficients and electron ranges in various materials can be found in the references.[45,46]

If the energy spread of the beam is small enough so that the scintillator response energy dependence does not have to be considered, then the scintillator-photodiode yields a signal proportional to the ion flux. In this case, the ion current pulse can be determined from this signal and the total number of ions per pulse measured by nuclear activation or some other technique. This technique has been successfully employed in a number of experiments at the U.S. Naval Research Laboratory.[3-4,47]

IV. BIASED ION COLLECTOR (BIC)

Charge collectors or Faraday cups have been used very successfully during the last few years to measure the current of intense, pulsed relativistic electron beams. Secondary electron currents are conveniently

22

suppressed by the negative space charge that is developed by the electrons in front of the collecting surface.

Determination of the current of intense ion beams by charge collectors is considerably more complicated than for relativistic electron beams. As stated previously, the main reason is that ion beams are space charge and current neutralized. The negative voltage required to repel the low energy electrons that accompany an ion beam also removes the secondary electrons from the surface of the collector resulting in an overestimation of the ion current. The error in measuring the current may be significant because of the large secondary electron emission. The secondary electron emission coefficient for protons of 0.01 to 1 MeV energy is typically greater than unity at normal incidence and increases as $\sec\theta$, where θ is the angle measured with respect to the normal, for protons impacting on a polycrystalline target.[48] In general, only a fraction of these secondary electrons contributes to the ion current if their only path to ground is through the incoming beam. If the applied bias potential is large enough to repel all the primary electrons near the aperture (see Fig. 20.), neutralization of the beam in the gap between the collecting-surface and the aperture is accomplished by the secondary electrons. This requires a secondary electron flux that is about equal to the ion flux, resulting in an overestimation of the ion current by a factor of two. The error may be even higher because of the contribution of ions from a plasma sheath at the aperture.

At rather low ion current density, secondary electrons can be easily suppressed by applying a magnetic field parallel to the collecting surface.[47,49] It has been demonstrated experimentally[47] that these

23

collectors (BIC - MES = Biased Ion Collectors with Magnetic Electron Suppression) are very reliable diagnostic too for low current ion beams. It is very doubtful that BIC - MES devices are as reliable for measuring the ion current of recently developed very intense beams because of the space charge effects. It should be pointed out that the radial space charge electric field of a 10^{13} cm^{-3} density ion beam at a radial distance of 1 mm is about 10^6 V/cm.

A typical Biased-Ion-Collector[47,50] is shown in Fig. 20. It consists of the collecting surface that is connected to the bias circuit, and a grounded electrostatic shield. The incoming beam enters through a small hole (aperture) in the front plate. The size of the aperture must be small in order for the induced signal to be very small in comparison with the applied potential. The side walls at the collecting surface are necessary, in particular when the device is used in the presence of an axial magnetic field. These side walls prevent the large gyroradius ions from striking the walls of the electrostatic shield and the insulator, thereby forming plasma that provides a path from the collecting surface to ground. This phenomenon has been observed repeatedly in the laboratory and it is manifested by output waveforms that last considerably longer than the ion pulse.

Thus, although the Biased-Ion-Collectors are simple and convenient devices for measuring ion-current densities, their results should be evaluated with extreme care. For absolute measurements, calibration (by comparison with an absolute measurement by a different technique) is necessary for the energy range and current density of interest. In general, these devices are more useful for relative than for absolute

measurements (e.g., to determine the radial profile), because even in the absence of all other drawbacks they are unable to discriminate between various ion species.

REFERENCES

1. S. Humphries, Jr., J.J. Lee and R.N. Sudan Appl. Phys. Lett., 25 (1974) 20.

2. J. Golden, C.A. Kapetanakos, S.J. Marsh, and S. Stephanakos, submitted to Phys. Rev. Lett.

3. S. Stephanakis, D. Mosher, et al., submitted to Phys. Rev. Lett.

4. J. Golden, F.C. Young and C. A. Kapetanakos, Bull. Am. Phys. Soc., 20 (1975) 583; J. Golden, C.A. Kapetanakos and S.A. Goldstein, Proc. 7th European Conf. on Controlled Fusion and Plasma Physics, Lausanne, Switz., (1975) 91; J. Golden, C.A. Kapetanakos, R. Lee and S.A. Goldstein, Proc. of the Int. Topical Conf. on Electron Beam Res. and Technology, Albq., N.M., Vol. I (1975) 635; C. A. Kapetanakos, J. Golden, W. M. Black, Phys. Rev. Lett. 37, 1236 (1976); and F. C. Young, Bull. Am. Phys. Soc. 20 (1975) 1294.

5. D. Demirlioglu and W. Whaling, Cal. Inst. Tech. (1962) Unpublished; W. Whaling, Handbuch der Physik, 34 (1958) 195.

6. J.B. Marion and F.C. Young, Nuclear Reaction Analysis, North Holland Pub. Co., Amsterdam (1968) 12.

7. F. Ajzenberg-Selove, Nucl. Phys. A152 (1970) 1.

8. J.D. Seagrave, Phys. Rev. 84 (1951) 1219.

9. F. Riess, P. Paul, J.B. Thomas and S.S. Hanna, Phys. Rev. 176 (1968) 1140.

10. D.F. Hebbard and G.M. Bailey, Nucl. Phys. 49 (1963) 666.

26

11. R.B. Day and T. Huss, Phys. Rev. 95 (1954) 1003.

12. G.B. Chadwick et al., Can. J. Phys. 34, (1956) 381.

13. S.E. Hunt, R.A. Pope and W.W. Evans, Phys. Rev. 106 (1957) 1012.

14. F. Ajzenberg-Selove, Nucl. Phys. A248 (1975) 1.

15. W.H. Burke, J.R. Risser and G.C. Phillips, Phys. Rev. 93 (1954) 188.

16. J.B. Marion, T.W. Bonner and C.F. Cook, Phys. Rev. 100 (1955) 847.

17. K. Wohlleben and E. Schuster, Radiochimica Acta 12 (1969) 75.

18. E. Schuster and K. Wohlleben, Intn. J. Appl. Rad. Isotopes 19 (1968) 471.

19. F.C. Young and M. Friedman, J. Appl. Phys. 46 (1975) 2001.

20. J. Csikai and G. Peto, Phys. Lett. 4 (1963) 252.

21. T. Retz-Schmidt and J. Weil, Phys. Rev. 119 (1960) 1079.

22. T.W. Bonner, J.E. Evans and J.E. Hill, Phys. Rev. 75 (1949) 1398.

23. T.W. Bonner, J.E. Evans, J.C. Harris and G.C. Phillips, Phys. Rev. 75 (1949) 1401.

24. R.J. Jaszczak, R.L. Macklin and J.H. Gibbons, Phys. Rev. 181 (1969) 1428.

25. C.L. Bailey, G. Freier and J.H. Williams, Phys. Rev. 73 (1948) 274.

26. J. Golden and C.A. Kapetanakos, Appl. Phys. Letts. 28 (1976) 3.

27. W.M. Latimer and J.H. Hildebrand, Eds., Reference Book of Inorganic Chemistry, Macmillian Co., NY (1964).

28. A.S. Ganeev et al., in Nuclear Reactions in Light Nuclei, Suppl 5 of Atomnaya Energiya, Moscow (1957) 21.

29. A. Hanson et al. Rev. Mod. Phys. 21 (1949) 635.

30. J.H. Gibbons and R.L. Macklin, Phys. Rev. 114 (1959) 571.

31. J.H. Gibbons and R.L. Macklin, Phys. Rev. <u>137</u> (1965) B1508.

32. G.J.F. Legge and I.F. Bubb, Nucl. Phys. <u>26</u> (1961) 616.

33. W. Gruhle, W. Schmidt and W. Burgmer, Nucl. Phys. <u>A186</u> (1972) 257.

34. J. Wing and J.R. Huizenga, Phys. Rev. <u>128</u> (1962) 280.

35. J.D. Kington <u>et al</u>., Phys. Rev. <u>99</u> (1955) 1393.

36. C.H. Johnson <u>et al</u>., Phys. Rev. <u>109</u> (1958) 1243.

37. F.C. Young and S.J. Stephanakis, Memo Report 3104, Naval Research Laboratory, Aug. 1975.

38. R.B. Theus, W.I. McGarry and L.A. Beach, Nucl. Phys. <u>80</u> (1966) 273.

39. N. Ying <u>et al</u>., Nucl. Phys. <u>A206</u> (1973) 481.

40. H.M. Kuan and J.R. Risser, Nucl. Phys. <u>51</u> (1964) 518.

41. F.M. Lanzafame and M. Blann, Nucl. Phys. <u>A142</u> (1970) 545.

42. J.J. Ramirez and L.W. Kruse, Rev. Sci. Inst. <u>47</u> (1976) 832.

43. D.L. Smith <u>et al</u>., Nuc. Inst. and Meth. <u>64</u> (1968) 157.

44. L.C. Northcliffe and R.F. Schilling, Nucl. Data Tables <u>A7</u> (1970) 233.

45. W.J. Veigele <u>et al</u>., Report DNA-2433F, Vol. 1, Kaman Sciences Corporation, Colorado Springs, Colorado (1971)

46. M.J. Berger and S.M. Seltzer, Report NASASP3012, NASA, Washington, D.C., (1964).

47. C.A. Kapetanakos, J. Golden and F.C. Young, Nucl. Fusion <u>16</u> (1976) 151.

48. G. Carter and J.S. Colligon, <u>Ion Bombardment of Solids</u>, American Elsevier Pub. Co. (1968) 67.

49. S. Humphries <u>et al</u>., J. Appl. Phys. <u>47</u> (1976) 2382.

50. C. Eichenberger <u>et al</u>., Report 188, LPS, Cornell Univ. (1976).

			Product Half-Life	Useful Energy Range
Beam	Target	Reaction		
Protons	^{10}B	^{10}B$(p,\gamma)^{11}$C$(\beta^+)^{11}$B	20.4 m	E_p = 1.145 MeV (resonance)
	^{12}C	^{12}C$(p,\gamma)^{13}$N$(\beta^+)^{13}$C	9.96 m	E_p = 457 keV (resonance)
				E_p = 1.70 MeV (resonance)
	^{14}N	^{14}N$(p,\gamma)^{15}$O$(\beta^+)^{15}$N	122 sec	E_p = 277 keV (resonance)
				E_p = 1.06 MeV (resonance)
Deuterons	^{10}B	^{10}B$(d,n)^{11}$C$(\beta^+)^{11}$B	20.4 m	E_d > 250 keV
	^{12}C	^{12}C$(d,n)^{13}$N$(\beta^+)^{13}$C	9.96 m	E_d > 600 keV
	^{14}N	^{14}N$(d,n)^{15}$O$(\beta^+)^{15}$N	122 sec	E_d > 700 keV

TABLE I. Proton and Deuteron Induced Reactions Producing Useful Positron Activity

TABLE II. Resonances and Thick Target Yields for the $^{14}N(p,\gamma)^{15}O$ Reaction

E_r (MeV)	Γ_{Lab} (keV)	Y_∞ (N) $\left(\dfrac{^{15}O/10^{10}}{\text{protons}}\right)$	Y_∞ (BN) $\left(\dfrac{^{15}O/10^{11}}{\text{protons}}\right)$	Total Y_∞ (BN) $\left(\dfrac{^{15}O/10^{11}}{\text{protons}}\right)$
0.278	1.5 ± 0.5	0.205	1.15	1.15
1.062	3.9 ± 0.7	8.56	47.9	49.1
1.55	34	1.27	7.11	56.2
1.742	4 ± 1	1.62	9.07	65.2
1.806	4.2 ± 0.4	3.91	2.19	67.4

30

TABLE III. The Yield of $^{10}B(p,\gamma)^{11}C$ for a Thick BN Target

E (MeV)	$\sigma(E)$ (μb)	ϵ(BN) (10^{-15} eV-cm²)	Y_p ($^{11}C/10^{11}$ protons)
0.4	0.2	16.7	0.0225
0.6	0.65	12.9	0.139
0.8	1.65	10.6	0.525
1.0	2.80	9.2	1.39
1.14	3.50	8.4	2.29
1.2	3.30	8.07	2.81
1.4	2.1	7.33	4.11
1.6	1.2	6.69	4.99
1.8	1.0	6.15	5.63

TABLE IV. Yield of the ^{10}B(d,n)^{11}C Reaction for a Thick BN Target

E (MeV)	σ (mb)	ε(BN) (10^{-15} eVcm^2)	Y_d(^{11}C/deuteron)
0.3	3.5	28.2	1.2 × 10^{-9}
0.4	7.7	25.0	5.45 × 10^{-9}
0.5	18.8	22.1	1.68 × 10^{-8}
0.6	36.1	19.9	4.30 × 10^{-8}
0.7	61.4	18.2	9.38 × 10^{-8}
0.8	87.5	16.7	1.78 × 10^{-7}
0.9	113	15.5	3.01 × 10^{-7}
1.0	128	14.4	4.60 × 10^{-7}
1.1	145	13.6	6.51 × 10^{-7}
1.2	161	12.8	8.79 × 10^{-7}
1.3	179	12.3	1.14 × 10^{-6}
1.4	197	11.6	1.33 × 10^{-6}
1.5	218	11.1	1.69 × 10^{-6}
1.6	237	10.6	2.10 × 10^{-6}
1.7	255	10.2	2.57 × 10^{-6}
1.8	276	9.8	3.09 × 10^{-6}

TABLE V. Yield of the $^{14}N(d,n)^{15}O$ Reaction for a Thick BN Target

E(MeV)	Y_d($^{15}O/10^7$ deuterons)
0.5	0.0016
0.6	0.014
0.7	0.12
0.8	0.25
0.9	0.57
1.0	1.04
1.1	1.67
1.2	2.5
1.3	3.4
1.4	4.6
1.5	5.9
1.6	7.4
1.7	9.0
1.8	10.7
1.9	12.5

TABLE VI. Thick Target Yield of the
$^{13}C(d,n)^{13}N$ Reaction on a Carbon Target

E (MeV)	σ (barns)	ε $(10^{-15}eV\text{-}cm^2)$	Relative Yield $\left(\dfrac{^{13}N/10^6}{deuterons}\right)$	Absolute Yield $\left(\dfrac{^{13}N/10^6}{deuterons}\right)$
0.40	0.00036	12.7	0.0010	0.0069
0.52	0.00327	11.2	0.020	0.014
0.64	0.0106	9.8	0.102	0.071
0.80	0.05	8.5	0.659	0.457
0.90	0.12	7.9	1.70	1.18
1.0	0.09	7.3	3.06	2.12
1.1	0.12	6.9	4.53	3.14
1.2	0.145	6.5	6.50	4.51
1.3	0.19	6.2	9.12	6.33
1.4	0.13	5.8	11.7	8.12
1.5	0.15	5.6	14.2	9.85
1.6	0.18	5.3	17.2	11.9
1.7	0.15	5.2	20.3	14.1
1.8	0.205	4.9	23.8	16.5
2.0	0.230	4.6	32.9	22.8
2.2	0.250	4.3	43.6	30.3
2.4	0.180	4.0	53.8	38.5

TABLE VII. Neutron-Producing Reactions for Ion Diagnostics

Reaction	Threshold Energy (MeV)	Typical Values		Reference
		σ(mb)	E(MeV)	
$D(d,n)^3He$	--	97	1	28,29
$^9Be(p,n)^9B$	2.06	100	2.5	30
$^9Be(d,n)^{10}B$	--			
$^9Be(\alpha,n)^{12}C$	--	200	2.0	30,31
$^{11}B(p,n)^{11}C$	3.0	150	3.5	32
$^{12}C(d,n)^{13}N$	0.33	120	0.9	22,23
$^{14}N(d,n)^{15}O$	0.14	15	1.5	20,21
$^{16}O(d,n)^{17}F$	1.83	500	5.0	33
$^{63}Cu(p,n)^{63}Zn$	4.21	250	6.6	34,35
$^{65}Cu(p,n)^{65}Zn$	2.17	175	4.5	34,35,36

TABLE VIII. Properties of (p,n) Reactions for Proton Diagnostics

Reaction	Threshold Energy (MeV)	Half-Life of Residual Nucleus	Energy of Delayed γ-Ray (MeV)	Reference for Cross Section
$^{11}B(p,n)^{11}C$	3.0	20.4 min	0.51	32
$^{14}N(p,n)^{14}O$	6.35	122 sec	2.31	40
$^{52}Cr(p,n)^{52m}Mn$	5.8	21.4 min	1.43	34
$^{63}Cu(p,n)^{63}Zn$	4.2	38.5 min	0.51	34
$^{65}Cu(p,n)^{65}Zn$	2.2	243.7 days	1.115	34

TABLE IX. Properties of Deuteron-Induced

Reactions for Diagnosing Deuterons

Reaction	Natural Isotopic Abundance of Target (%)	Half-Life of Residual Nucleus (min)	Energy of Delayed Y-Ray (MeV)
$^{12}C(d,n)^{13}N$	98.89	9.97	0.51
$^{27}Al(d,p)^{28}Al$	100	2.24	1.78
$^{51}V(d,p)^{52}V$	99.75	3.76	1.43

TABLE X. Properties of (α,xn) Reactions on Gold

Reaction	Half-Life of Residual Nucleus (hr)	Energy of Delayed γ-Ray (keV)	No. of Photons per Decay
$^{197}\text{Au}(\alpha,\text{n})^{200}\text{Tl}$	26.1	367.9	0.88
$^{197}\text{Au}(\alpha,2\text{n})^{199}\text{Tl}$	7.42	455.0	0.13
$^{197}\text{Au}(\alpha,3\text{n})^{198m}\text{Tl}$	1.87	283.0	0.26
$^{197}\text{Au}(\alpha,4\text{n})^{197}\text{Tl}$	2.84	152.2	0.075
$^{197}\text{Au}(\alpha,5\text{n})^{196}\text{Tl}$	1.40	695.5	1.0

TABLE XI. Ratios of Proton Ranges in Polymers to the

Range in Aluminum Calculated by the Bragg-Kleeman Rule

Polymer	Density (g/cm^3)	R/R_{Al}
Polycarbonate (Kimfol) $(C_{12}H_{14}O_3)_n$	1.34	1.21
Polyester (Mylar) $(C_{10}H_8O_4)_n$	1.39	1.22
Methyl Methacrylate (Plexiglas) $(C_5H_8O_2)_n$	1.18	1.32
Polyethylene $(CH_2:CH_2)_n$	0.94	1.42
Polystyrene $(C_6H_5CH:CH_2)_n$	1.04	1.46
Polyamide (Kapton) $(C_{22}H_{10}N_2O_4)_n$	1.11	1.56
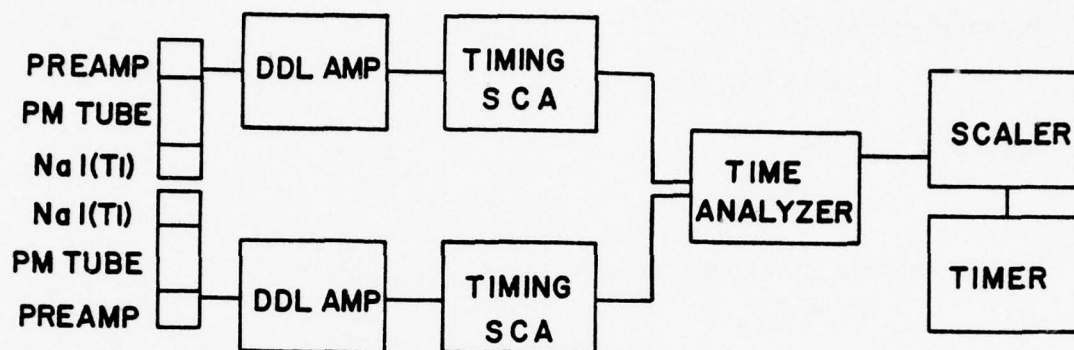
Fig. 1 — Coincident gamma-ray detection apparatus
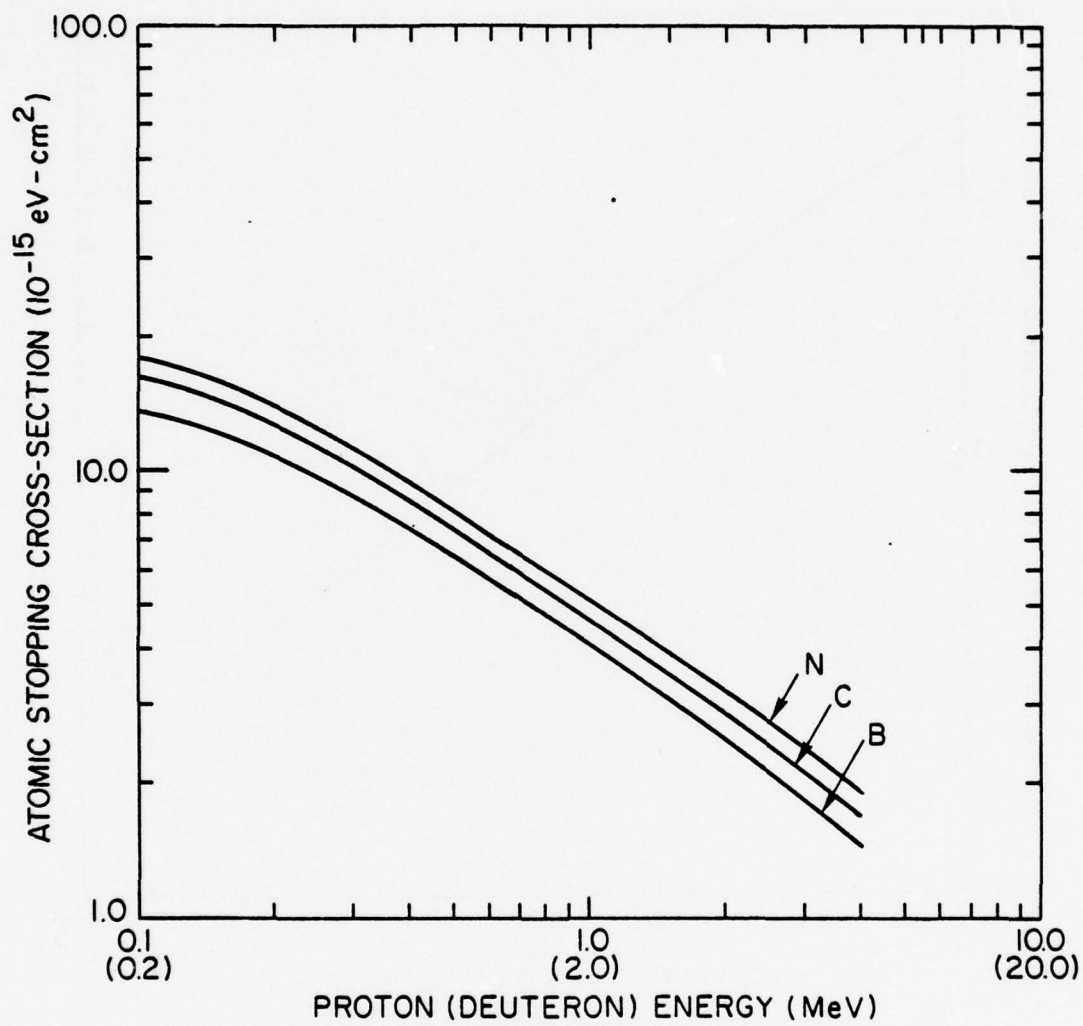
Fig. 2 — Stopping cross-sections for boron, carbon and nitrogen[5]

41

ATOMIC STOPPING CROSS-SECTION (10^{-15} eV - cm^2)

10.0

1.0

0.1

H

0.1
(0.2)

1.0
(2.0)

10.0
(20.0)

PROTON (DEUTERON) ENERGY (MeV)
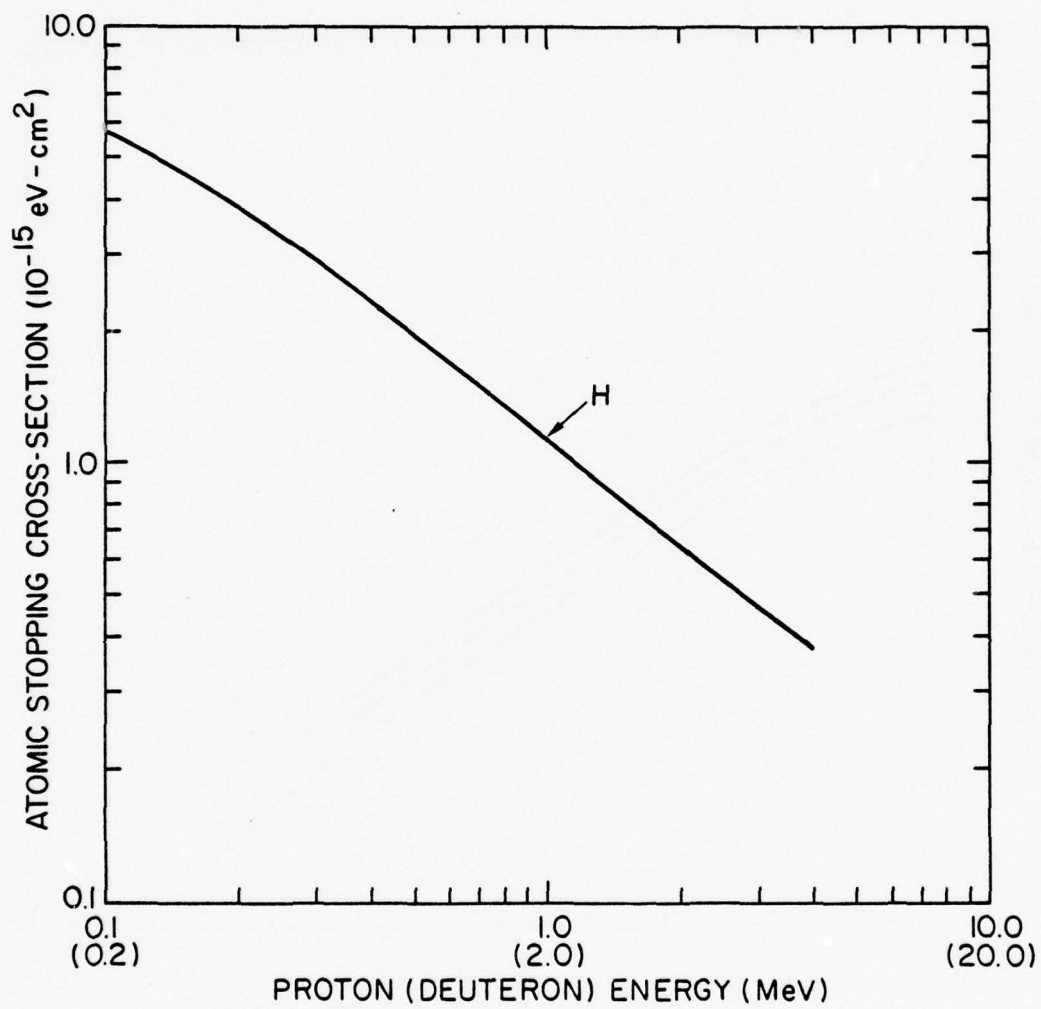
Fig. 3 — Stopping cross-sections for hydrogen[5]

42
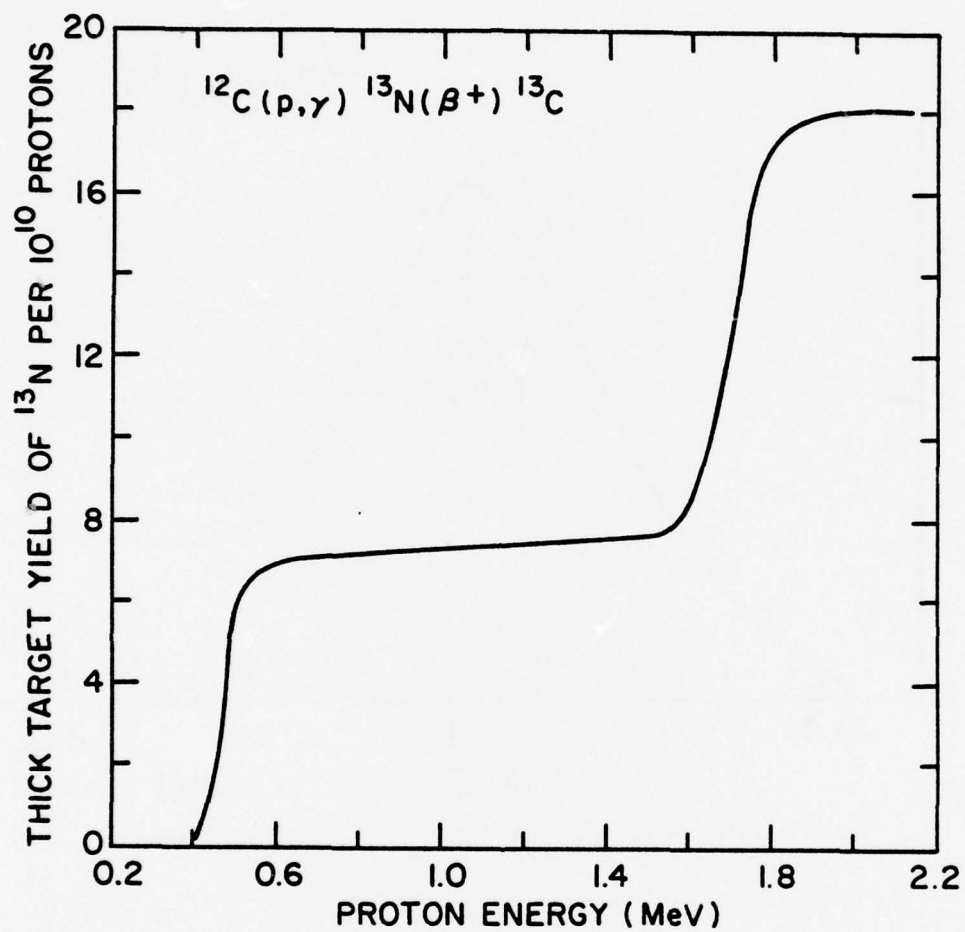
Fig. 4 — Thick target yield of the $^{12}C(p, \gamma)^{13}N(\beta^+)^{13}C$ reaction[8]
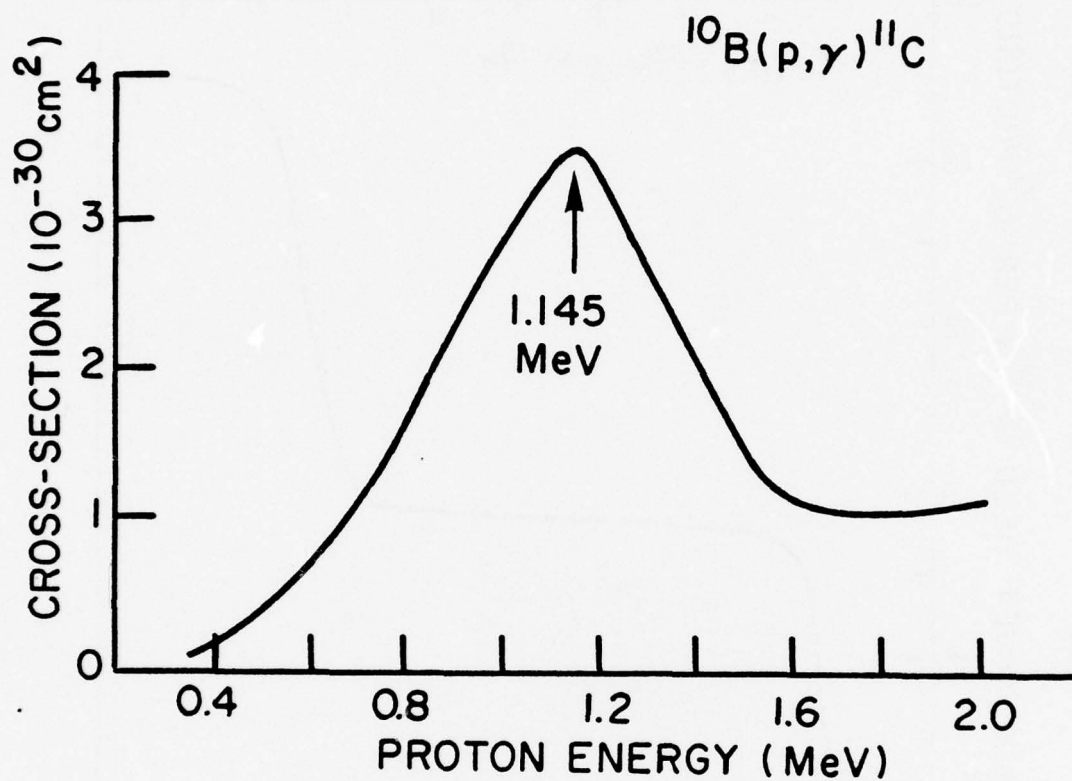
Fig. 5 — Cross-sections for the $^{10}B(p, \gamma)^{11}C(\beta^+)^{11}B$ reaction[12]
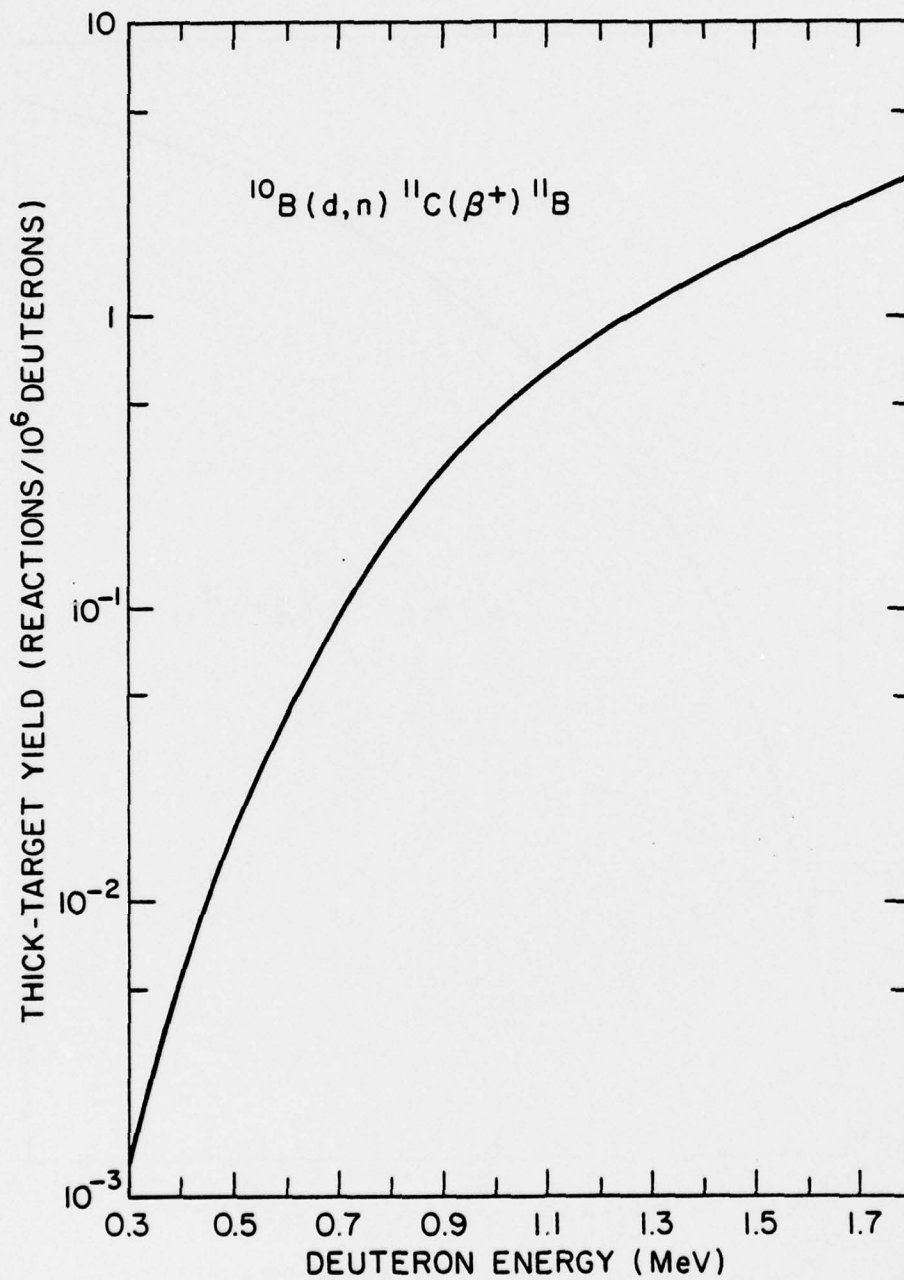
Fig. 6 — Yield of the $^{10}B(d, n)^{11}C$ reaction for a thick BN target
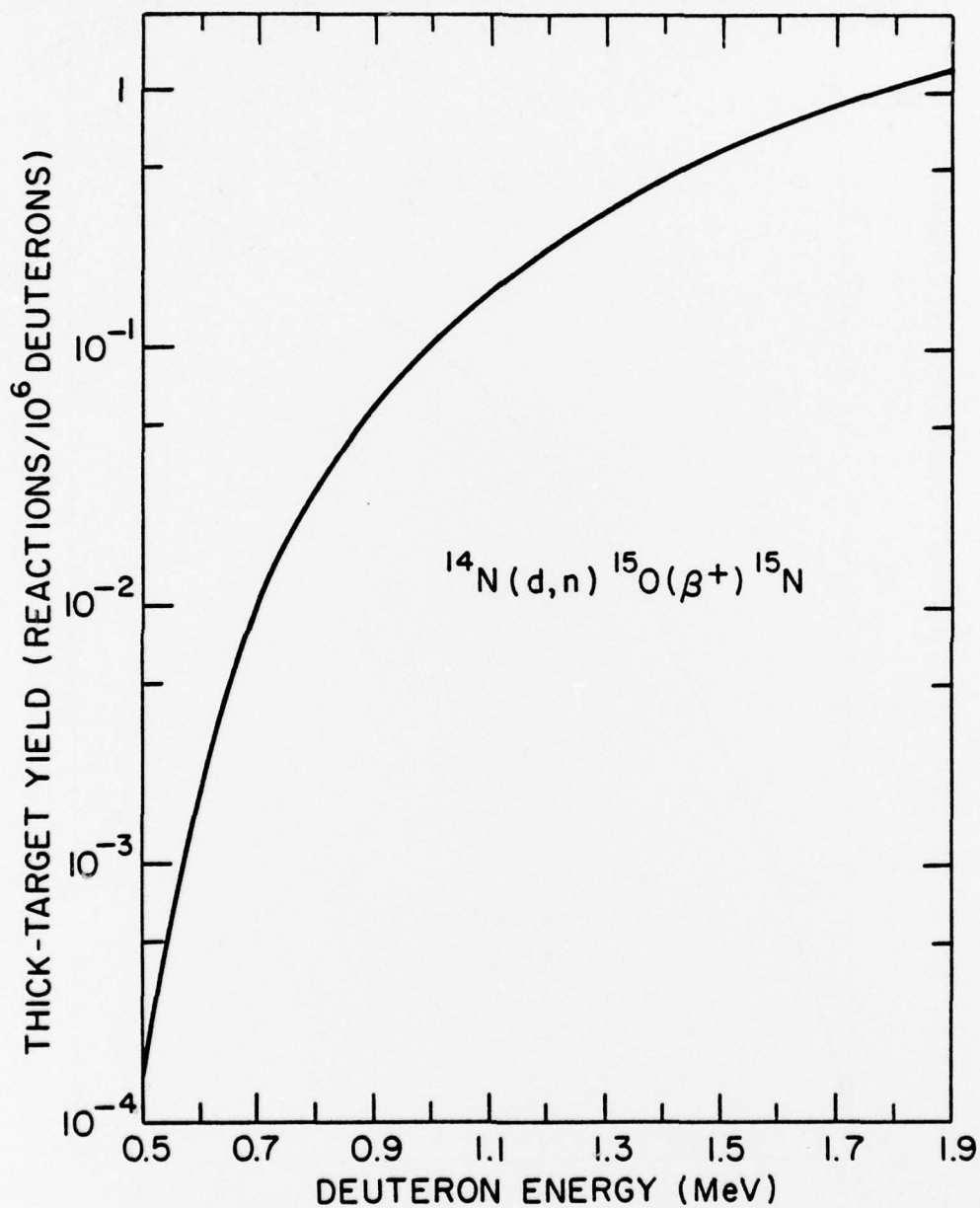
Fig. 7 — Yield of the $^{14}N(d, n)^{15}O(\beta^+)^{15}N$ reaction for a thick BN target
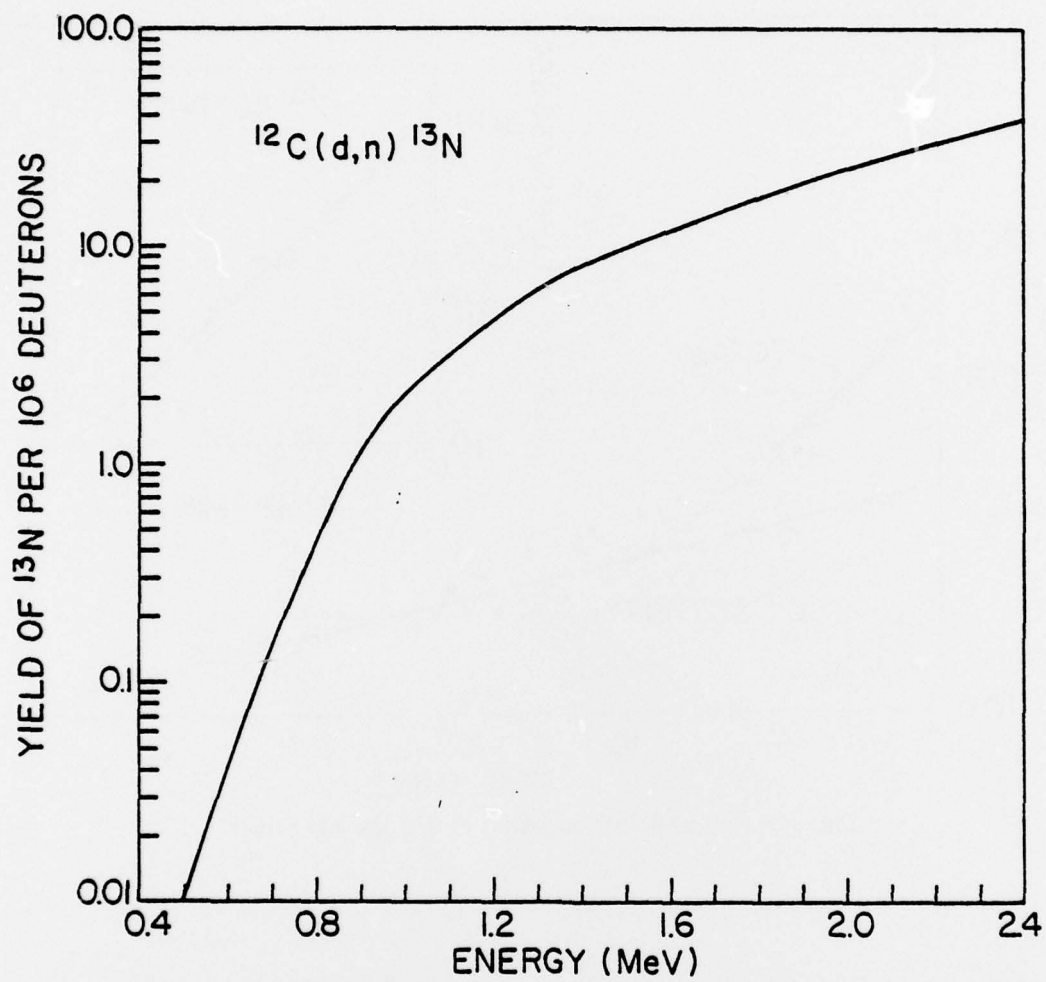
Fig. 8 — Thick target yield for the $^{12}C(d, n)^{13}N(\beta^+)^{13}C$ reaction
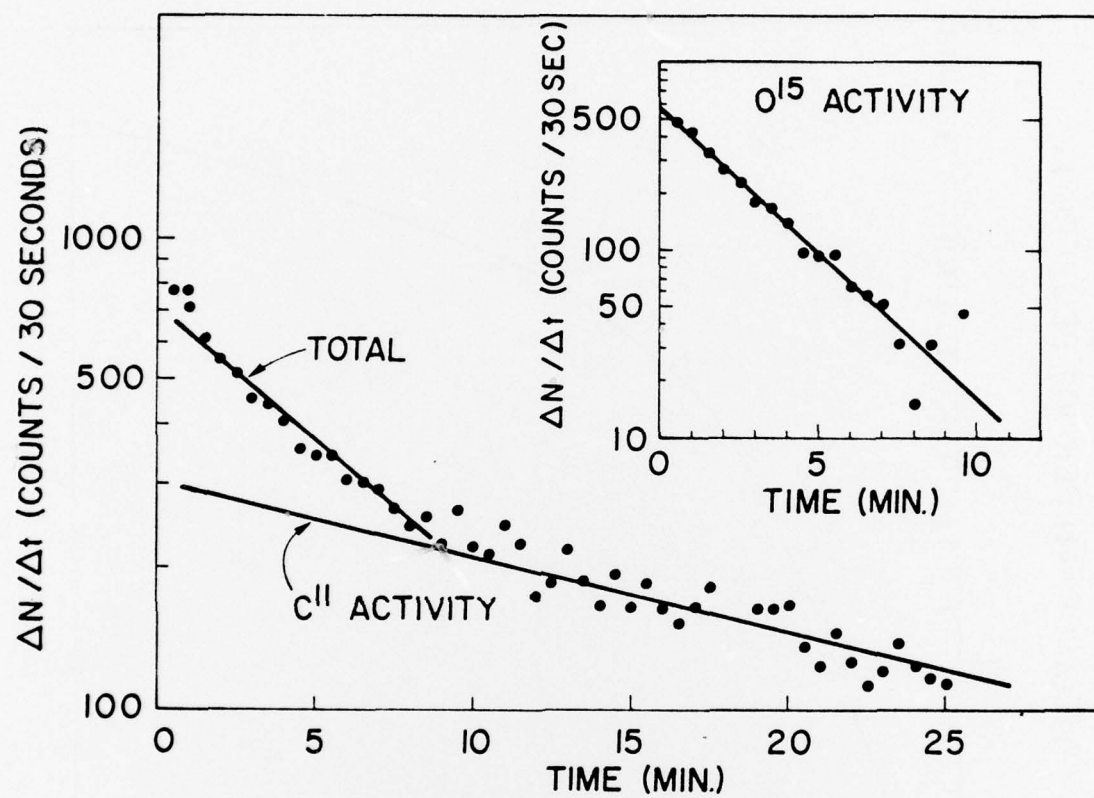
Fig. 9 — ^{11}C and ^{15}O activities in a thick BN target
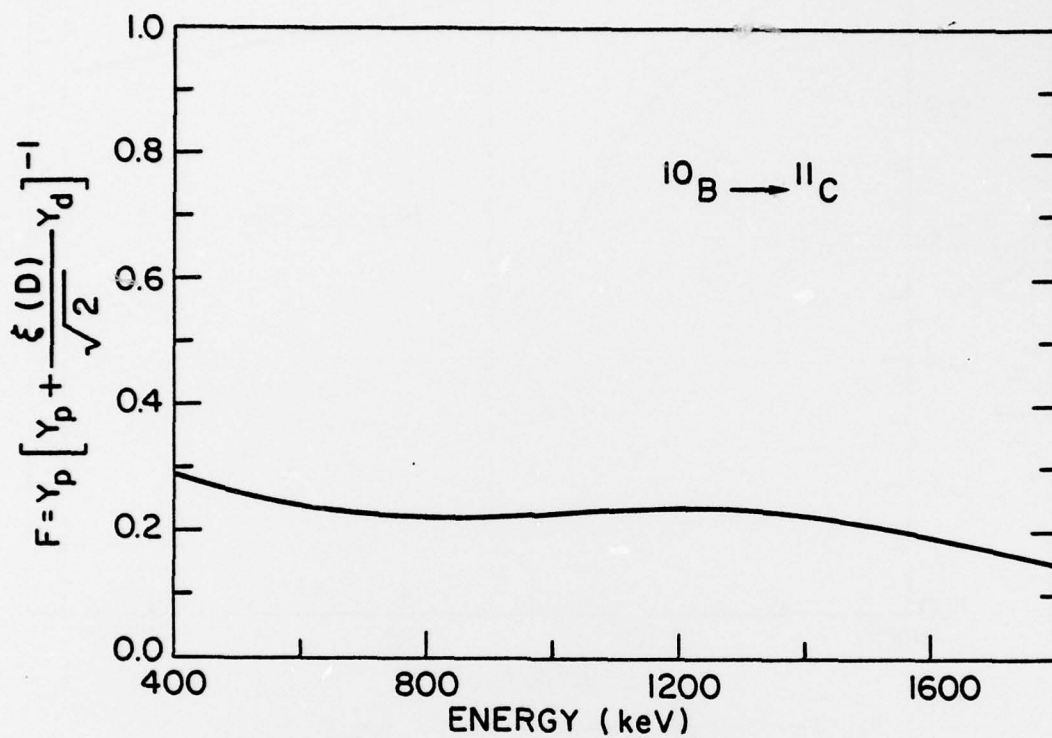
Fig. 10 — Deuteron correction factor, F, for $^{10}B \rightarrow ^{11}C$
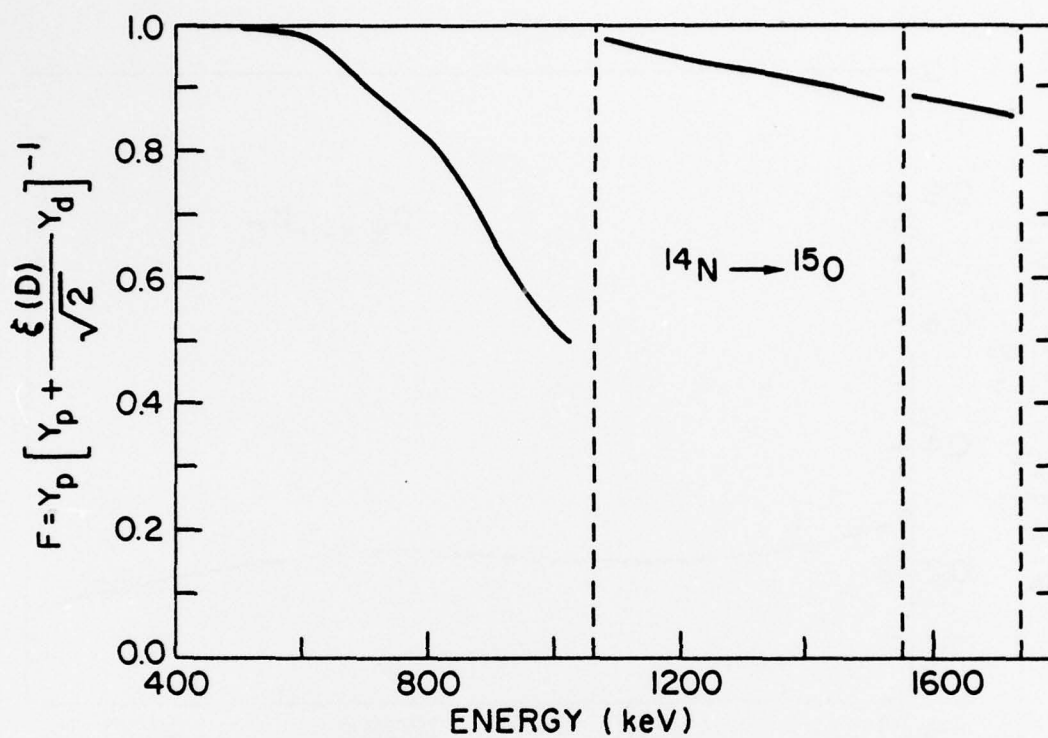
Fig. 11 — Deuteron correction factor, F, for $^{14}N \rightarrow {}^{15}O$
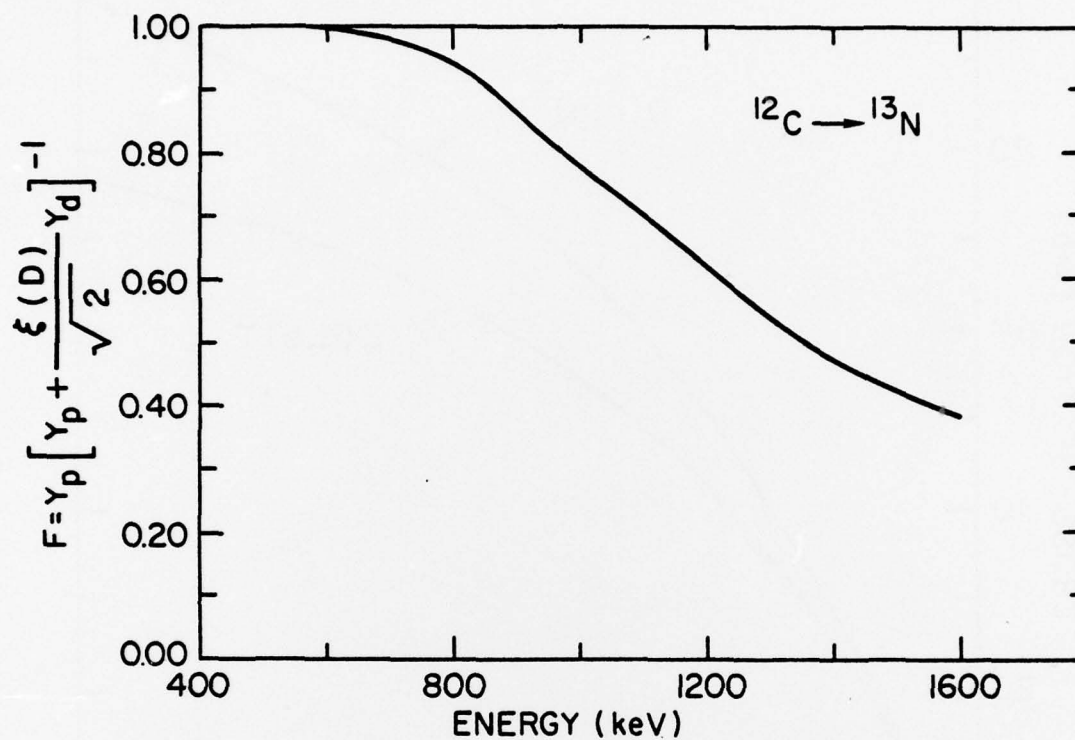
Fig. 12 — Deuteron correction factor, F, for $^{12}C \rightarrow ^{13}N$
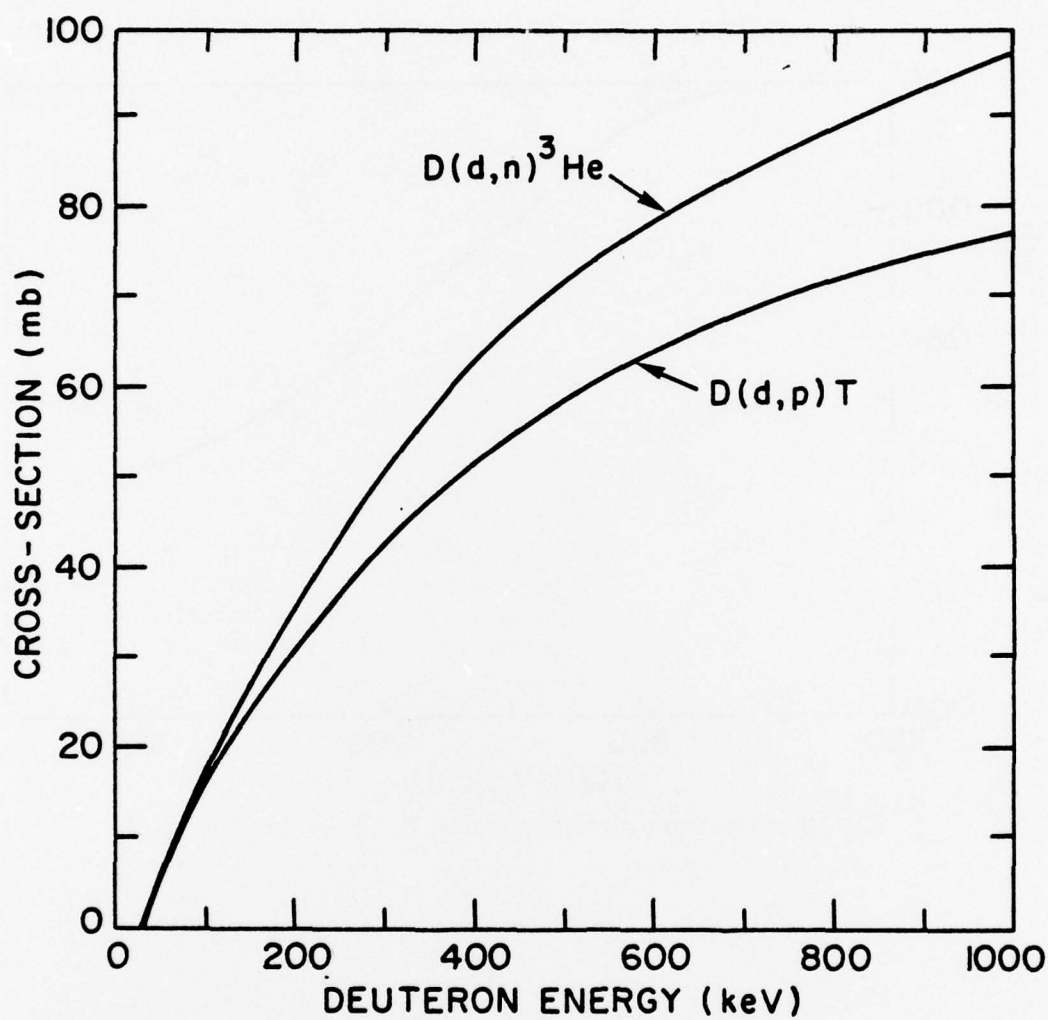
Fig. 13 — Cross-sections for D-D reactions
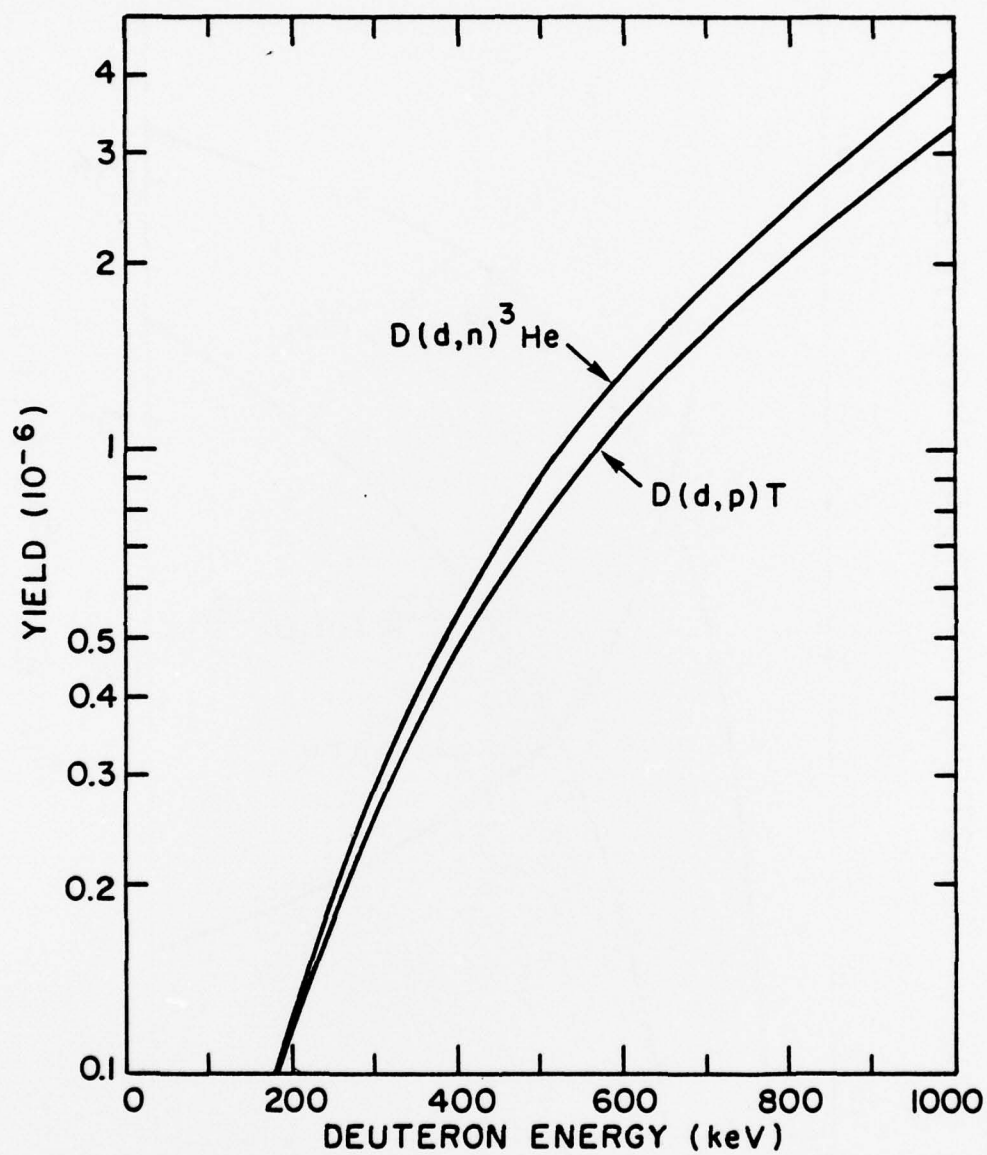
Fig. 14 — Thick target yields for D-D reactions (CD$_2$ target)
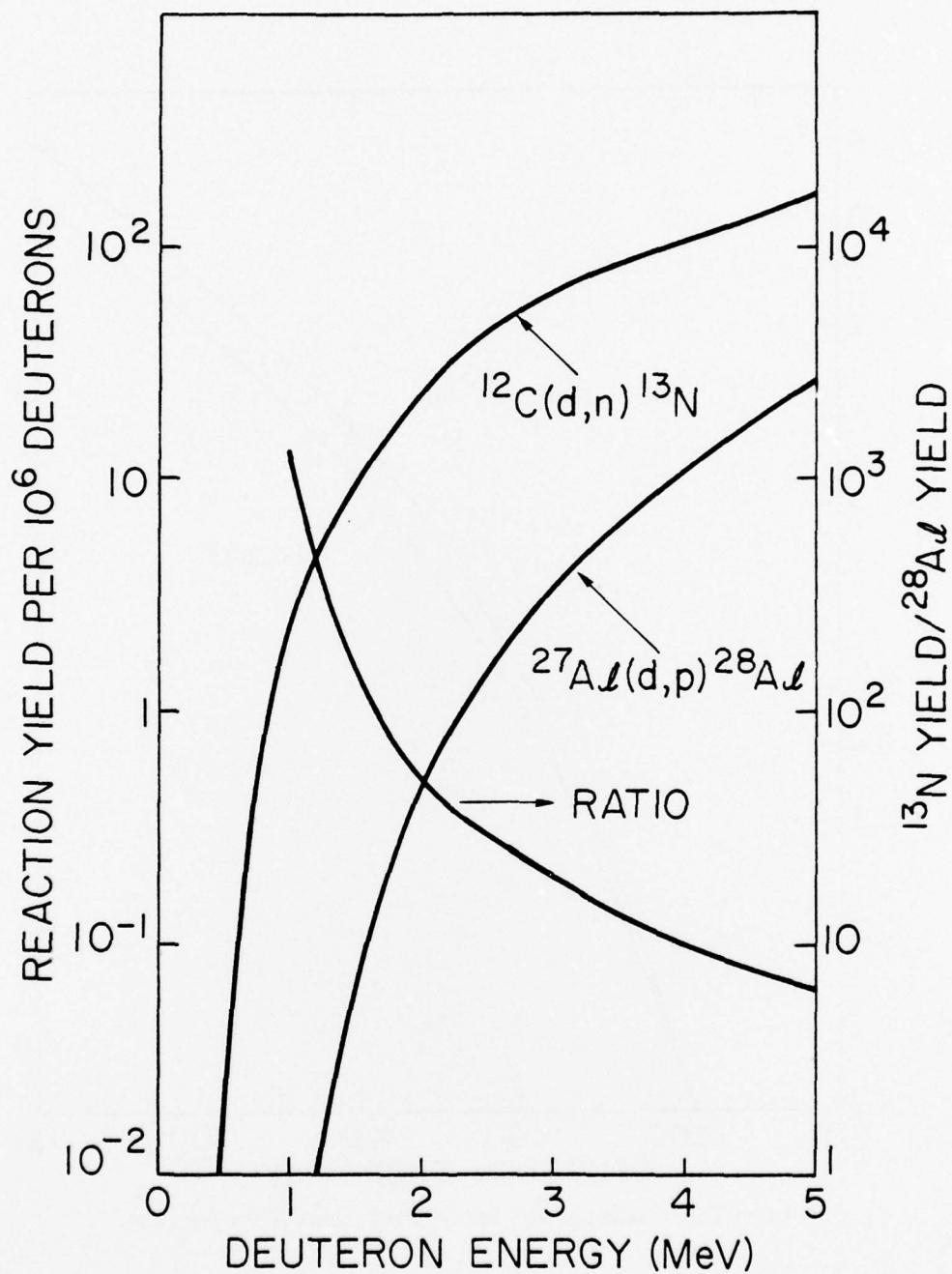
Fig. 15 — Thick target yields for the $^{12}C(d, n)^{13}N$ and $^{27}Al(d, p)^{28}Al$ reactions and their ratios

54
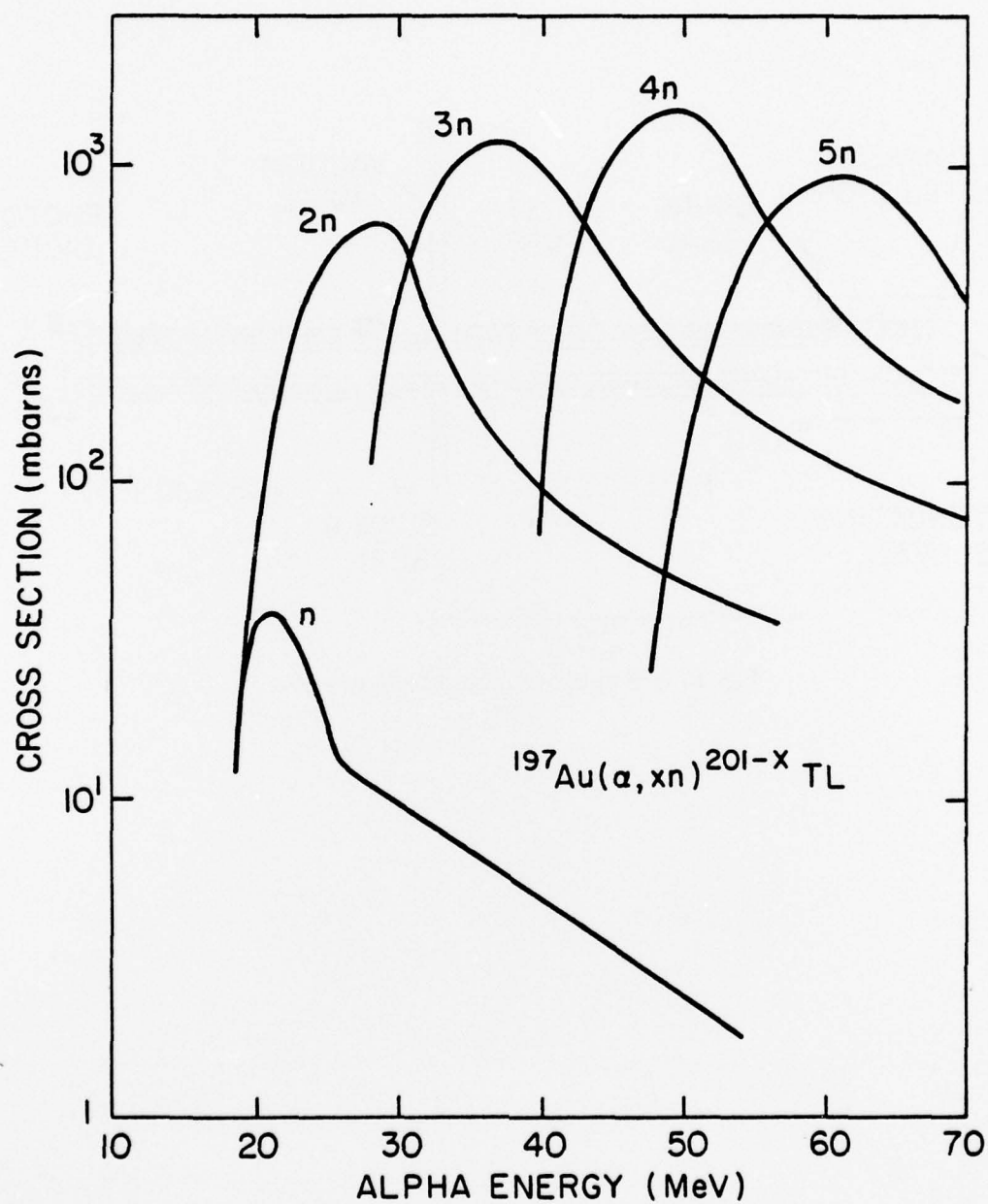
Fig. 16 — Cross-sections for the ^{197}Au$(\alpha, xn)^{201-x}$Tl reactions
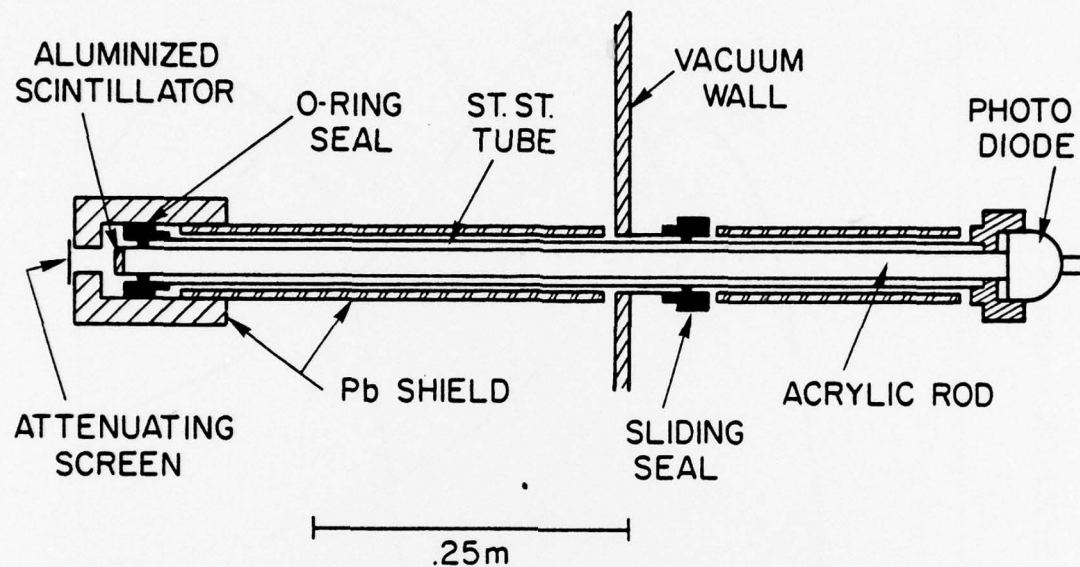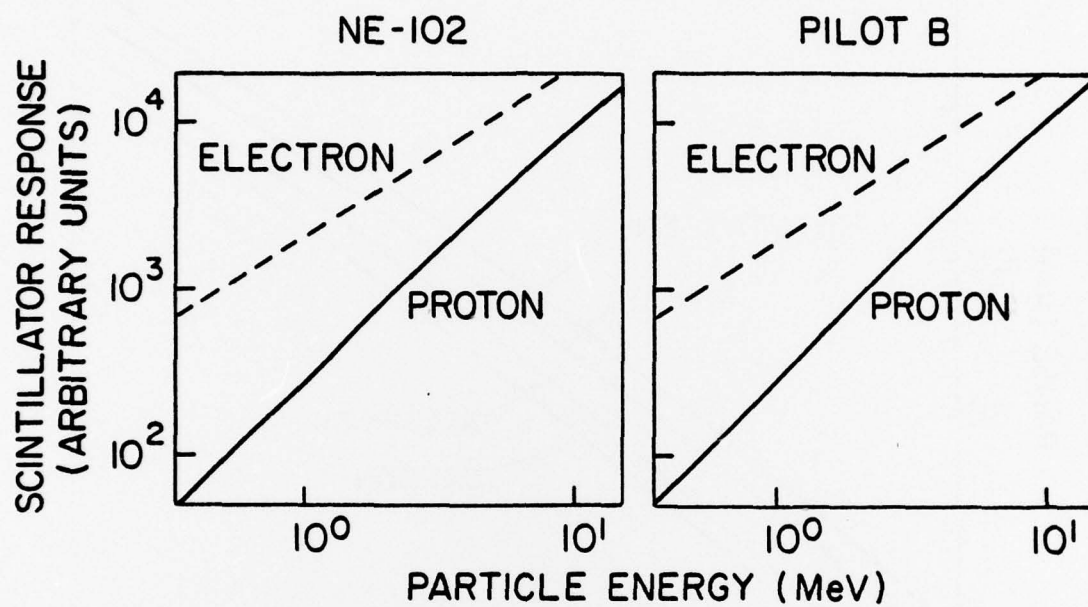
Fig. 17 — Scintillator-photodiode detector

56

NE-102   PILOT B

Fig. 18 — Response of plastic scintillator to electrons and protons[43]

57

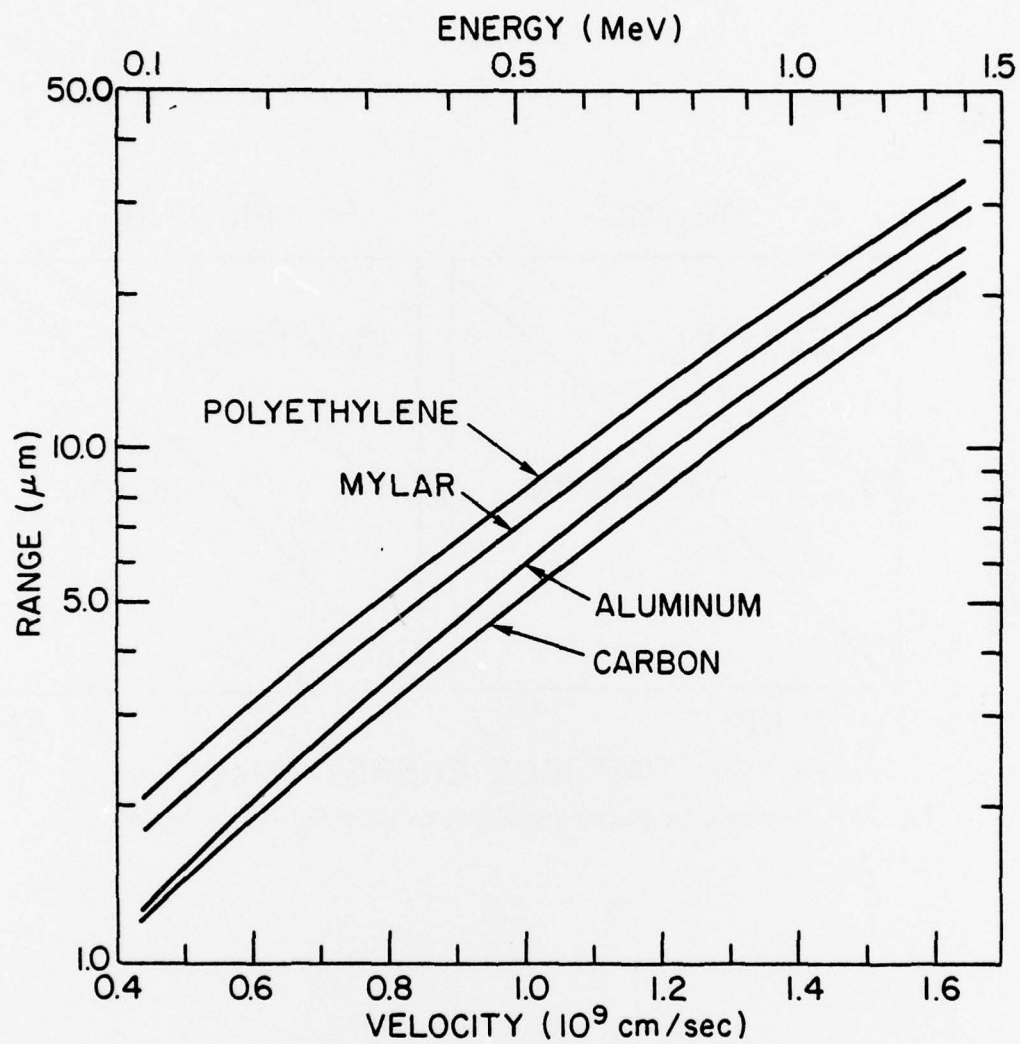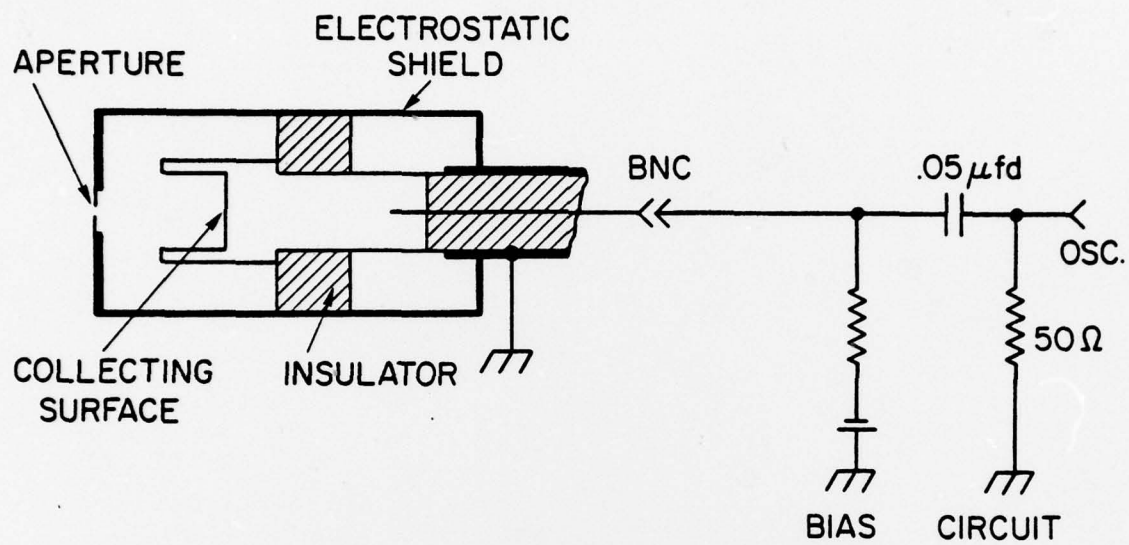Fig. 19 — Proton range in various materials[44]

58

Fig. 20 — A typical biased-ion-collector